GREEN SYNTHESIS OF Cu_2O NANOPARTICLE USING *PRUNUS CERASIFERA* FOR PHOTOCATALYTIC REDUCTION OF Cr (VI)

BY:

MASRESHA TEFERA

ADVISOR

NEWAY BELACHEW (Ph.D.)

Debre Berhan University
College of Natural and Computational Science
Department of Chemistry

THESIS SUBMITTED TO DEPARTMENT OF CHEMISTRY, DEBRE BERHAN UNIVERSITY, DEBRE BERHAN FOR THE PARTIAL FULFILMENT OF THE DEGREE OF MASTER OF SCIENCE IN CHEMISTRY

Feb, 2021

Debre Berhan, Ethiopia

APPROVAL SHEET

Debre Berhan University

College of Post Graduate Studies

Department Of Chemistry

This is to certify that the thesis prepared by Masresha Tefera, entitled "Green synthesis of Cu_2O nanoparticle using *prunus cerasifera* for photocatalytic reduction of Cr (VI)" and submitted in partial fulfillment of the requirements for the degree of "Master of Science in Chemistry" complies with the regulation of the university and meets the accepted standards with respect to originality and quality.

Signature of Board of Examiners

External examiner _____ signature _____ date _____

Internal examiner _____signature _____ date _____

Advisor _____ signature _____ date _____

DECLARATION

I the under signed, declare that this thesis is my original work and has not been presented for degree in any other university and that all source of materials used for the thesis have been duly acknowledged.

Name Masresha Tefera

Signature _____

Department Chemistry

Date __/__/2021

ACKNOWLEDGEMENT

First of all, my greatest debt of gratitude is owed to my Almighty God for his daily guidance and care out my life. Without his and his mother abundant mercies and meticulous help, I would not reach this stage.

I would like to express my sincere gratitude and appreciation to my advisor, Neway Belachew (Ph.D.), for his unlimited and constructive guidance, advice, suggestions, comments and friendly approach during the course of this work. I thank him from the bottom of my heart for all his deeds that are difficult to express in words.

My thanks also go to the Chemistry Department of Debre Berhan University for allows me to use laboratory apparatus, instruments and chemicals during my experimental work.

I would also like to thank all the Chemistry Department laboratory technicians of the Debre Berhan University in general and to Mr. Hirpo Hinsene in particular for his time and help during my experimental work.

My deepest gratitude also goes to my father Tefera Yihunie who always sacrificed in all the matter and dream to see my success and well-being and also for his endless effort and contribution. I am also grateful to my mother Yenewub Yizengaw who has done her level best to see my success. Again I want to express my gratitude to my brothers, my sisters and my homologue, intimate friend Gize Mekuriaw for their unreserved help and support.

Last but not least, I express my gratefulness for all who directly or indirectly contributed to the successful completion of the study and the write up of the thesis.

TABLE OF CONTENTS

Contents **Page**

LIST OF FIGURES

Figures **Page**

LIST OF TABLES

Tables **Page**

LIST OF ABBREVIATIONS

A	Absorbance
Ac	Alicyclic
ANOVA	Analysis of variance
l	Cell length
CV	Coefficient of variation
R	Correlation coefficient
DF	Degree of freedom
EDTA	Ethylenediaminetetraacetate
FT-IR	Fourier transform infrared
FWHM	Full width at half maximum
GA	Gallic acid
g	gram
mg	miligram
mL	milliliter
ε	Molar absorptivity
NC	Nanocomposite
NPs	Nanoparticles
NP	Nitro Phenol
PNP	Para Nitro Phenol
ppm	parts per million
pH	potential of hydrogen
P-XRD	Powder X-ray diffraction
RDA	Recommended Dietary Allowances
RSM-BBD	Response surface methodology coupled with Box-Behnken design
SEM-EDS	Scanning electronic microscopy/Energy dispersive X-ray spectroscopy
SD	Standard deviation
UV-Vis	Ultra Violet- Visible Spectrophotometer
VIF	Variance inflation factor
λ	Wavelength
ZPC	Zero Point charge

ABSTRACT

In this study, the reported is environmentally friendly, cost-effective, and single-step procedure is used for a successful green synthesis of cuprous oxide (Cu_2O) by using prunus cerasifera plant from a precursor salt, $CuCl_2.2H_2O$. Prunus cerasifera extract solution has contained Gallic acid, which is a good capping or reducing agent for the reduction of dihydrated copper chloride to Cu_2O nanoparticle. The Cu_2O nanoparticle was characterized by FT-IR spectroscopy and powder XRD. The Nano sized cuprous dioxide (Cu_2O) nanoparticles were used for the photocatalytic reduction of hexavalent chromium. Hexavalent chromium Cr (VI) pollution makes has a harmful impact on human health and the ecological environment. Photocatalysis reduction technology exhibits low energy consumption, high reduction efficiency and stable performance, and is playing an increasingly important role in chromium pollution control. Ultra violet cabinet has been used to reduce Cr (VI) to the less harmful Cr (III) due to its visible light catalytic activity, easily available, chemical stability and low cost photoreduction of hexavalent chromium, Cr (VI), identified as carcinogenic and mutagenic element, to Cr (III), believed to be an essential element, using cuprous dioxide (Cu_2O) nanostructures as photocatalyst was investigated under visible light irradiation. The reduction of Cr (VI) in aqueous solution by visible light/ Cu_2O was studied under various variables, pH, contact time and concentration of hexavalent chromium.

Keywords: *Prunus cerasifera*, cuprous oxide, Photocatalytic reduction, Hexavalent chromium

1 INTRODUCTION

1.1 Background

Nanotechnologies are a booming business. It is now evident that nanotechnologies are becoming a substantial part of society and indeed already a multitude of nanotechnology products, or at least products with a nano-based claim, are commercially available. Nanotechnologies include the development and production of nanosized engineered particles, fibers, coatings, etc., collectively referred to as nanomaterials. Nanomaterials are defined as materials composed of unbound particles or as particles in an aggregate or agglomerate state with one or more external dimensions with a size ranging from 1 to 100 nm. Such materials possess typical nanostructure-dependent properties (e.g., chemical, biological, optical, mechanical, and magnetic), which distinguish them from their bulk counterparts. Because of their new and unique properties, nanomaterial's are becoming ubiquitous in various products, such as sunscreens, cosmetics, medical supplies, clothing, and building materials.[1]

Nanomaterials are cornerstones of Nanoscience and nanotechnology. Nanostructure science and technology is a broad and interdisciplinary area of research and development activity that has been growing explosively worldwide in the past few years. It has the potential for revolutionizing how materials and products are created and the range and nature of functionalities that can be accessed. It is already having a significant commercial impact, which will assuredly increase in the future.[2]

Clean water is one of the most important elements for all living organisms to sustain life. However, due to the rapid pace of industrialization and tremendous increase in the population, the contamination of water resources has occurred globally.[3]

However, synthesis of nanostructured materials using a facile and environmental benign approach is a prime concern of the scientific community. A synthesis of these materials with tailored properties such as high surface area is also demands further investigations in the field. Hence, it is highly desirable to introduce facile and greener synthesis techniques of nanomaterials for various technological applications.

1.2 Statement of the problem

During the last decades, a huge amount of polluted water has been discharged from various industries bringing anxiety for the sustainability of life. The emerging water pollutants such as pharmaceuticals, pesticides, fertilizers, and toxic heavy metals are becoming a threat to humankind. Toxic metals heavy metals (Pb (II), Hg (II), Cd (II), and Cr (VI)) even at a very low concentration can disrupt the normal metabolic activity of mammals. Among these metals, chromium is widely used in various industries, universities, and research centers. More importantly, chromium is widely used in tanning industries as cross-linking the collagen fibers for enhancing the strength of leather. It is in mind that, tanning factories in Ethiopia are found in almost every part of the country. Therefore, it has been expected to release a huge quantity of Cr contaminated water to the sounding environment.[4, 5]

Chromium can be found in stable Cr (VI) or Cr (III) oxidation states. More importantly, Cr (VI) is considered the most toxic form of Cr, which usually exists in association with oxygen as chromate (CrO_4^{2-}) or dichromate ($Cr_2O_7^{2-}$) oxyanions. Cr (III) is less toxic and less mobile and is mainly found bound to the organic matter in the aquatic environments and soil. The Agency for Toxic Substances and Disease Registry classifies Cr(VI) as the top 16th hazardous substance due to its severe toxicity [6]. The maximum value of chromium intended for human consumption is estimated as 0.1 mg L^{-1} [7]. Therefore, the removal of Cr (VI) from water bodies is of prime importance. Adsorption, fluctuation, segmentation, and photocatalytic reduction to less toxic forms are widely used for the removal of dye. Photocatalytic reduction of Cr (VI) currently takes a substantial interest for a competent approach. But it is hard to get suitable semiconductor material for efficiently utilizing solar radiation from the visible region.

The synthesis of Cu_2O nanoparticles using synthetic chemicals hampers its sustainability and practical application. Hence introducing inexpensive and less toxic chemicals to the environment, humans, and aquatic organisms is an issue. The use of phytochemical extracts for the syntheses of nanostructured materials provides a new alternative to the synthesis of nanostructured materials. Herein, *Prunus cerasifera* fruit extract solution as a cost-effective, less toxic, and environmentally friendly reducing agent. To the best of our knowledge, there is no report on utilizing *Prunus cerasifera* fruit extract for the synthesis of Cu_2O nanoparticles.

1.3 Objectives of the study

1.3.1 General objective

The general objective of the study is to synthesize Cu_2O nanoparticles using *Prunus cerasifera* fruit extract as a reducing agent for photocatalytic reduction of the toxic Cr (VI) to Cr (III).

1.3.2 Specific objectives

The specific objectives of the study are:

- To synthesize Cu_2O nanoparticle using *Prunus cerasifera* fruit extract as a reducing agent
- To investigate the structure and composition of Cu_2O nanoparticles synthesis using powder XRD and FTIR.
- To investigate the photo catalytic efficiency of Cu_2O nanoparticles by the reduction Cr (VI) to Cr (III).

1.4 Significance of the study

There is a non-stop increase in environmental pollution (industrial, atmospheric, aquatic, and agricultural, etc.). To overcome this pollution, introducing highly efficient and sustainable photo catalysts has brought a promise to confront the problem. Hence, our photo catalyst provides a competitive efficiency for combating water pollutants, especially organic dyes and Cr (VI) reduction. Besides, the study contributes to the scientific community by introducing an alternative synthesis of Cu_2O using *Prunus cerasifera* fruit juice extract for the first time.

2 LITERATURE REVIEW

2.1 Introduction to nanoparticles

Nanoparticles are ultrafine units with dimensions measured in nanometers (as shown in Figure 2.1 below). Nanoparticles exist in the natural world and are also created as a result of human activities. Because of their submicroscopic size, they have unique material characteristics, and manufactured nanoparticles may find practical applications in a variety of areas, including medicine, engineering, catalysis, and environmental remediation. A natural, incidental, or manufactured material containing particles, in an unbound state or as an aggregate or as an agglomerate and where, for 50% or more of the particles in the number size distribution, one or more external dimensions is in the size range 1 nm–100 nm.[8]

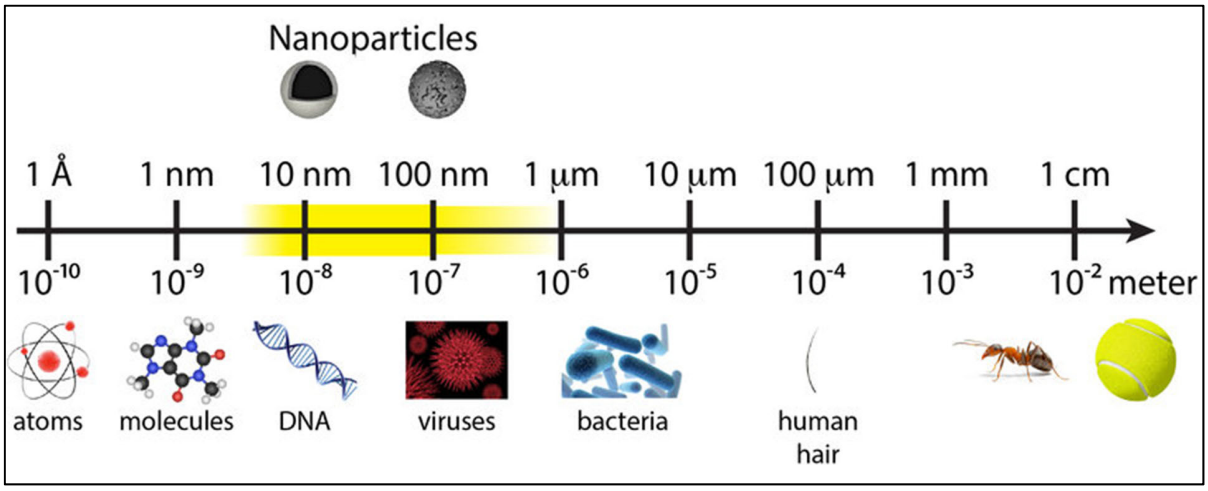

Figure Error! No text of specified style in document.**.1** One dimension of a nanomaterial should be in the 1-100 nm range. As a comparison, other typical sizes of everyday objects and organisms are shown.

That size range from 1 to 100 nm overlaps considerably with that previously assigned to the field of colloid science from 1 to 1,000 nm which is sometimes alternatively called the mesoscale. Thus, it is not uncommon to find literature that refers to nanoparticles and colloidal particles in equal terms. The difference is essentially semantic for particles below 100 nm in size.[8]

Nanoparticles can be classified into many various types, according to their size, shape, and material properties. Nanomaterials based on their dimension are generally grouped into four categories (Figure 2.2). Nanoparticles based on the dimension they are zero-dimensional (0D),

confined below 100 nm in all 3 dimensions. Some classifications distinguish between organic and inorganic nanoparticles; the first group includes dendrimers, liposomes, and polymeric nanoparticles, while the latter includes fullerenes, quantum dots, and gold nanoparticles. Other classifications divide nanoparticles according to whether they are carbon-based, ceramic, semiconducting, or polymeric. Besides, nanoparticles can be classified as hard (e.g. Titania [titanium dioxide], silica [silicon dioxide] particles, and fullerenes) or as soft (e.g., liposomes, vesicles, and Nano droplets). Nanoparticles are also further classified typically depends on their application, such as in diagnosis or therapy versus basic research, or maybe related to how they were produced.[9]

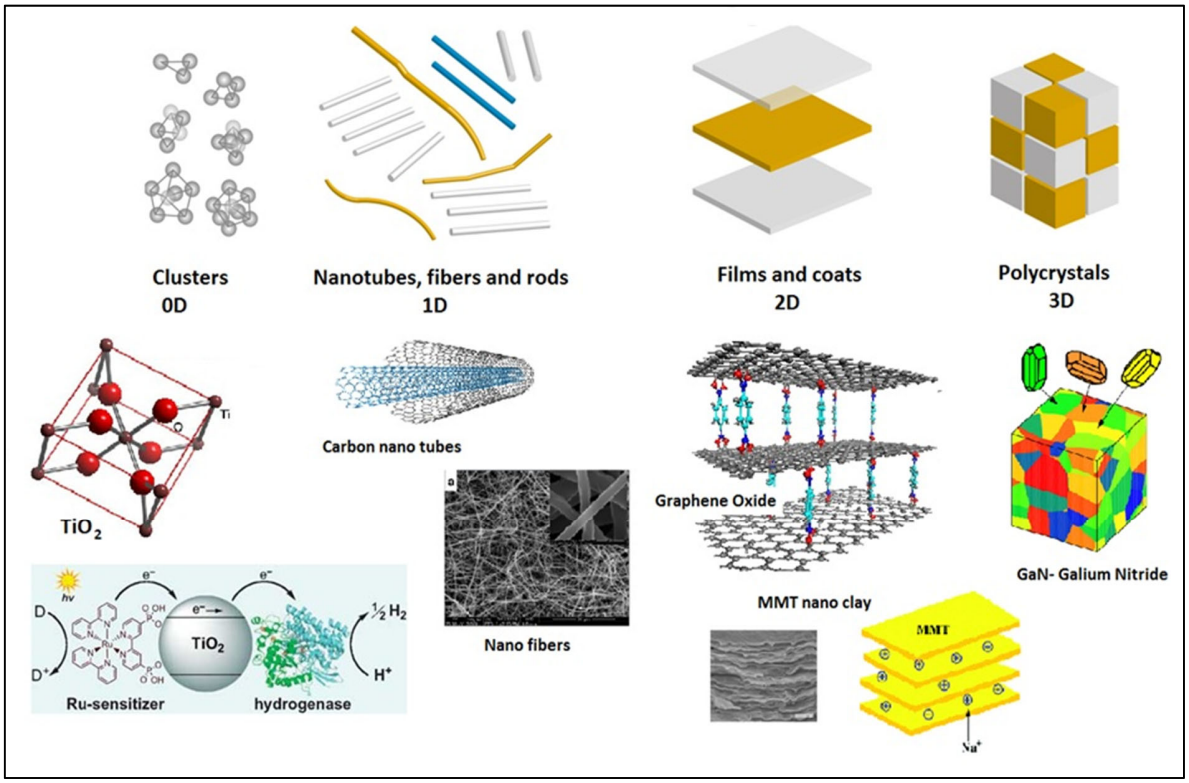

Figure Error! No text of specified style in document.**.2** The classification of nanomaterial's based on their confinement.

Cuprous oxide (Cu_2O) is a narrow band gap (2.17 eV), visible light active p-type semiconductor. There have been reported numerous works of literature on the efficiency of Cu_2O under visible light irradiation.[10, 11]

2.2 Structure and properties of Cu_2O NPs

Copper (I) oxide (cuprous oxide) is an inorganic compound with the chemical formula Cu_2O. Copper (I) oxide crystallizes in a cubic structure. It is easily reduced by hydrogen when heated. It undergoes disproportionation in acid solutions producing copper (II) ions and copper. When the cupric oxide is gently heated with metallic copper, it is converted into cuprous oxide. Cu2O acts as good corrosion resistance, due to reactions at the surface between the copper and the oxygen in the air to give a thin protective oxide layer.[12]

2.2.1 Structure of Cu_2O

The Cu_2O crystal structure is formed by two interpenetrating three-dimensional Cu_2O networks. This structure is stabilized by Cu–Cu inter-network interactions and Cu–O intra-network bonds [13]. Copper (I) Oxide structure (Cu_2O) seems like as shown below in Figure 2.3.[14]

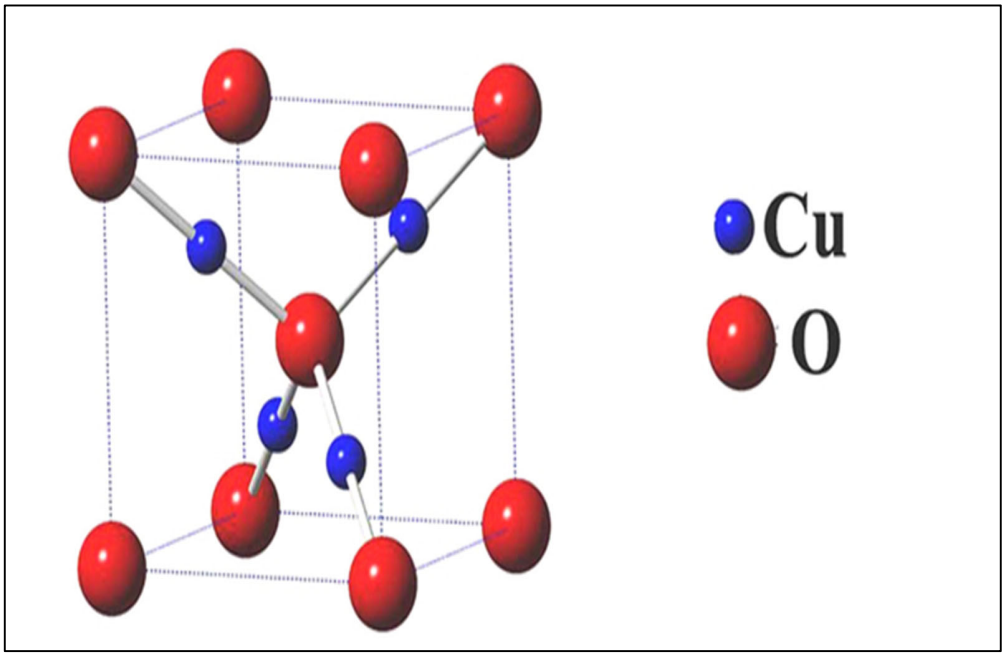

Figure Error! No text of specified style in document..**3** The structure of Cu_2O

2.2.2 Physical Properties of Copper (I) Oxide

Physical properties of Cu_2O stated in the table below in Table 2.1. [14]

Cu_2O	Copper (I) oxide
Density	6 g/cm^3
Molecular Weight/ Molar Mass	143.09g/mol
Boiling Point	1,800℃
Melting Point	1,232℃
Chemical Formula	Cu_2O
Odour	No odour
Appearance	Red coloured solid
Covalently bonded unit	3
Solubility	Insoluble in water
Lattice parameter (a)	4.27A°

Table Error! No text of specified style in document.**.1** Physical Properties of Copper (I) Oxide (Cu_2O)

2.2.3 Chemical Properties of Copper (I) Oxide

Copper (I) oxide reacts with water in the presence of oxygen forms copper (II) hydroxide. The chemical equation is given below;

$$2Cu_2O + 4H_2O + O_2 \rightarrow 4Cu(OH)_2$$

Copper (I) oxide reacts with hydrogen chloride forms Copper (I) chloride and water. The chemical equation is given below;

$$Cu_2O + 2HCl \rightarrow 2CuCl + H_2O$$

2.3 Different synthetic techniques of Cu_2O nanoparticle

Cuprous oxide (Cu_2O) has various characteristics due to the stoichiometric deviations arising from its preparation methods and parameters [15]. Cu_2O has been successfully synthesized by many methods including electrolysis, reduction of cupric salts or copper oxide, thermal oxidation, hydrothermal, mechanochemical approach and γ-irradiation methods [15, 16].

2.3.1 Hydrothermal/solvothermal

Hydrothermal synthesis a unique method for crystallizing substances from high-temperature aqueous solutions at high vapor pressures; also termed “hydrothermal method." The term “hydrothermal” is of geologic origin.[16]

Hydrothermal synthesis can be defined as a method of synthesis of single crystals that depends on the solubility of minerals in hot water under high pressure. The crystal growth is performed in an apparatus consisting of a steel pressure vessel called an autoclave, in which a nutrient is supplied along with water. A temperature gradient is maintained between the opposite ends of the growth chamber. At the hotter end the nutrient solute dissolves, while at the cooler end it is deposited on a seed crystal, growing the desired crystal.[16]

Cuprous oxide (Cu_2O) has been successfully synthesized by a hydrothermal method at 200 ^oC for 2 h using Cu $(CH_3COO)_2 \cdot H_2O$, glycine ($C_2H_5NO_2$) and NaOH. The morphology of Cu_2O is significantly influenced by the concentration of glycine or NaOH [17].

2.3.2 Mechanochemical approach

Mechanochemical synthesis is a processing technique of solids in which mechanical and chemical phenomena are coupled on a molecular scale. It is possible to produce a desired product using only a mechanical action (high pressure and mechanical stress between reactants and balls) at room temperature or at temperatures lower than traditional solid-state synthesis [18].

Mechanochemical synthesis can be performed under different conditions, e.g., using a reactive atmosphere (reactive ball milling [BM]), under cryogenic conditions (cryomilling), or in a solvent. In addition, other experimental parameters can be controlled that influence the characteristics of the final material: milling time, powder to ball weight ratio, milling temperature, milling frequency, milling atmosphere and pressure of the selected gas, etc. Depending on the synthesis parameters, different products can be obtained, such as metastable phases, high-pressure phases, and amorphous and disordered phases, leading to the development of ultrafine-grained and nanostructured compounds with homogeneous composition.[18]

The pure Cu powders are ground in chloride solutions by a planetary ball mill. Elemental Cu powders (5 g, 99.99%,–100 meshes) are selected as the raw material. Ball milling is carried out at 400rpm in the Cu container containing 100 ml $CuCl_2$ solution with different [Cl^-] concentration. The Cu balls with diameter of 15mm are used and the weight ratio of balls to powders is 20:1. The as-milled products are washed by distilled water and then dried in vacuum at 40 ◦C for 2 h. [19]

Although the exact mechanism and reaction route are not very clear yet, a series of reactions as follows are assumed during the whole process based on the present investigation results and previous research results [19]:

$$CuCl_2 + 2H_2O \rightarrow Cu(OH)_2 + 2HCl$$
$$CuCl_2 + Cu \rightarrow 2CuCl$$
$$Cu(OH)_2 + Cu \rightarrow 2CuOH$$
$$2CuOH \rightarrow Cu_2O + H_2O$$
$$CuCl_2 + 3Cu(OH)_2 \rightarrow 2Cu_2(OH)_3Cl$$
$$Cu(OH)_2 \rightarrow CuO + H_2O$$
$$CuO + Cu \rightarrow Cu_2O$$

The most essential reaction of all mentioned above is (i.e., $CuO + Cu \rightarrow Cu_2O$ (or $Cu + Cu^{2+} \rightarrow 2Cu^{+}$). And it should be noted that the reaction $CuCl_2 + 2H_2O \rightarrow Cu(OH)_2 + 2HCl$ is generally limited and the $CuCl_2$ cannot be hydrolyzed completely. Obviously, there are different reaction processes for various $CuCl_2$ solutions at different [Cl^-] concentrations, which were proved by different products and relative content in the different milling time. Moreover, it should be noted that the reaction $CuCl_2 + 3Cu(OH)_2 \rightarrow 2Cu_2(OH)_3Cl$ may be very weak or even not to occur when the [Cl^-] concentration is 0.75×10^{-2} mol/L because the $Cu_2(OH)_3Cl$ phase could not be found in the XRD patterns. Thus, it can be deduced that different [Cl^-] concentration would affect reactions during different milling periods, e.g., the reaction time for forming single phase Cu_2O and the size as well as shape of Cu_2O nanoparticles.

2.3.3 Co-precipitation method

Precipitation/co-precipitation is a standard synthesis technique to prepare pure/multinary metal oxide nanoparticles. In a typical co-precipitation reaction, a salt precursor, generally a nitrate, chloride, or oxy-chloride, is dissolved in aqueous solution and then the corresponding hydroxides

are precipitated by the addition of a base such as ammonium hydroxide or sodium hydroxide. After washing the produced ammonium or sodium salt, the hydroxides are calcined resulting in metal oxide powders. If more than one precursor salt is used in the starting solution, multinary metal oxides can be obtained by co-precipitation of the corresponding hydroxides. The control of particle size and distribution is difficult if the rate of precipitation is not slow (controlled); however, it was reported that nanosized metal oxide powder is synthesized with a modified co-precipitation method by keeping the pH level constant.[20]

Co-precipitation is the most commonly used method for the synthesis of magnetic nanoparticles. Pure iron oxides and ferrites, which are iron oxides chemically combined with one or more additional metals including Mn, Co, Cu, Mg, Zn, and Ni, are conveniently synthesized from aqueous solutions of metal salts by the addition of a base under oxygen-free atmosphere at either room or elevated temperature [20].

Co-precipitation reactions involve the formation of simultaneous nucleation, growth, coarsening, and/or agglomeration processes to take place. Co-precipitation reactions exhibit the following characteristic stages [21]:

i. The products are obtained as an insoluble species in supersaturating conditions.
ii. Nucleation process helps to form a large number of small particles.
iii. Post nucleation process takes place due to Ostwald ripening processes which lead to aggregation, dramatically affecting the particle size, shape, morphology, and, with other applications, properties.
iv. The super saturation help to induce precipitation at the reaction scale.

The Cu_2O nanoparticles were prepared by the following procedure. A 100 mL aqueous solution containing $CuSO_4.5H_2O$ (5 g), polyvinyl alcohol (4 g), and isopropanol (15 mL) as a reagent solution was stirred for 2 h. During the mixing, precipitator solution (NH_4OH) prepared in different places with various concentrations of 0.5 M, 0.75 M, and 1 M, and then precipitator was added drop wise to the reagent solution with vigorous stirring at room temperature. After 1 h of stirring, the precipitate particles were isolated from the solution by centrifugation at 6,000 rpm for 30 min and the solution changed into green-yellowish precipitates. The product was filtered using whatman paper, and then washed by aquabidest and absolute ethanol, respectively for three

times, to reduce impurities and decrease pH value of the filtrate. The final product was dried in oven at 80°C for 4 h [22].

2.3.4 Sol-gel method

Sol–gel processing makes possible the synthesis of solid products by gelation rather than by crystallization or precipitation. This process can be described as the creation of an oxide network by progressive polycondensation reactions of molecular precursors in a liquid medium, or as a process to form materials via a sol, gelation of the sol, and finally removal of the solvent. Publications dealing with sol–gel processing have appeared.[23]

The terms “sol” and “gel” are defined as follows. A sol is a stable suspension of colloidal solid particles or polymers in a liquid. The particles can be amorphous or crystalline. A gel consists of a porous, three-dimensionally continuous solid network surrounding and supporting a continuous liquid phase (“wet gel”). In “colloidal” (“particulate”) gels, the network is made by agglomeration of dense colloidal particles, whereas in “polymeric” gels the particles have a polymeric substructure resulting from the aggregation of subcolloidal chemical units. In general, the sol particles can be connected by covalent bonds, van der Waals forces, or hydrogen bonds. Gels can also be formed by entanglement of polymer chains. In most sol–gel systems used for materials syntheses, gelation (formation of the gels) is due to the formation of covalent bonds and is irreversible.[23]

Sol–gel processing proceeds in several steps: (i) hydrolysis and condensation of the molecular precursors and formation of sols; (ii) gelation (sol–gel transition); (iii) aging; and (iv) drying. There are different processing options leading from the sol to various materials. Powders can be obtained by spray-drying of a sol. Gel fibers can be drawn directly from the sol, or thin films can be prepared by standard coating technologies such as dip- or spin-coating, spraying, etc. [23]

The sol-gel synthesis of silica is based on the hydrolysis and condensation of silicon alkoxides M(OR)z where R is an alkyl group (R = Me, Et, Pr ...). Hydrolysis gives reactive silanol groups whereas condensation leads to the formation of bridging oxygen. [24]

$$\text{Si-OR} + H_2O \Rightarrow \text{Si-OH} + \text{ROH} \quad \text{(hydrolysis)}$$

$$\text{Si-OH} + \text{RO-Si} \Rightarrow \text{Si-O-Si} + \text{ROH} \quad \text{(condensation)}$$

The synthesis of cupric oxide and cuprous oxide nanoparticles by the sol-gel process is based on Cu $(CH_3COO)_2$, H_2O as a starting material. It has been reported that CuO and Cu_2O particles grow through the dehydration - condensation reaction of $Cu(OH)_2$ species [25].
Copper (II) acetate, ($Cu(C_2H_3O_2)_2$, 99.999 % purity) was used as starting material for the synthesis of cuprous oxide thin films. The details preparation of cuprous oxide thin film was published previously. Using a spin coater, the solution was transformed into thin film form. Indium tin oxide (ITO) coated glass was used as substrates. The coating rates used was 2000, 4000 and 6000 rpm and the coating time was set to 40 s for all films. 40 s of coating is sufficient for having the solution spreading completely onto substrate. The as-coated films were dried at 250 ºC in air for 15 min to evaporate the solvent. The process was repeated to produce two layers of coating. Films were annealed at 350 °C for 1 h in 5% H_2 + 95 % N_2 atmosphere. Annealing temperature 350 °C was found to be suitable for the formation of Cu_2O phase in hydrogen atmosphere. Since the higher annealing temperature would produce Cu phase [26].

2.3.5 Microwave irradiation

Microwave irradiation involves electromagnetic wave in the range of 300 MHz – 300 GHz. Typical microwave ovens or microwave reactors work at a frequency of 2.45 GHz. The microwave irradiation produces efficient internal heating by direct coupling of microwave energy with the molecules of biomass. The microwave radiation causes heating by two main mechanisms: dipolar polarization and ionic conduction. The heating depends on the ability of the materials being heated to absorb microwaves and convert it into heat. Metals, for example, reflect microwave, while biomass absorbs it.[27]

The microwave reactor is different from other indirectly heated reactors, whereas biomass particles are heated externally, that is, heat from the reactor wall arrives at the surface of biomass particles, and then it is conducted into the interior of the biomass. Contrary to this, biomass particles in a microwave reactor are heated from within. Microwave heating biomass may not be very efficient because biomass is a poor thermal conductor. In a microwave reactor, the heating is internal; every part of the biomass in the path of microwave radiation is heated simultaneously. Limited data available show that microwave torrefaction creates an extremely fast rate of heating of the biomass interior in a matter of seconds. So, it does not allow heat to be conducted adequately to its exterior, and it causes a large temperature gradient in wood sizes of 25 mm or

larger. Some investigators found more encouraging results including 67 % – 90 % energy yield with 79 % – 88 % overall energy recovery.[27]

Microwave irradiation method is a novel graphene synthesis method with fast processing time. This method uses a high-frequency wave to heat the starting materials (i.e., graphite, amorphous carbon, and other carbon sources) to a high temperature in a short time. The heating mechanism of microwave irradiation can be explained from two main processes, namely, dipolar polarization and ionic conduction.[28]

The intensity of electromagnetic radiation is commonly expressed in one of two ways. The maximum value of the oscillating electric field strength, Emax in volts per meter is given, or the energy flux, I, in watts per square meter, joules per square meter per second) is given. When dealing with microwave applications, the unit used is most often milliwatts per square centimeter. The intensity of radiation is proportional to the square of the maximum electric field intensity, which is called the amplitude to the wave. An easily remembered equality between these two ways of expressing the intensity of radiation is: $I = 1/2c\varepsilon_o E^2max$. Where c is the velocity of electromagnetic waves in vacuum (2.997×10^8 meters/sec.), ε_o is the permittivity of vacuum (8.854×10^{-12} Farads/meter) and Emax is the maximum electric field strength, or amplitude, of the wave in volts per meter. A typical comparison is that a microwave with an electric field amplitude of 1 volt/centimeter has an intensity of 1.328 milliwatts/square centimeter.[29]

Seven Cu_2O microcrystals were prepared. In a typical synthesis, 0.744 g EDTA $Na_2.2H_2O$ and 0.32 g NaOH were dissolved in 3.5 mL water followed by the addition of 0.11 g $Cu(Ac)_2.2H_2O$ and 6.5 mL n-butyl alcohol. The volumes of water and n-butyl alcohol were altered to produce different microcrystals. After sonication for 30 s, the solution was transferred into a microwave glass vessel. The vessel was then placed into a single-mode Microwave Synthesizer and irradiated for 15 min at 100 ˚C under magnetic stirring. The final Cu_2O products were filtered and washed with distilled water and ethanol three times each.[30]

Copper acetate and oxalic acid in 1:1 ratio were taken in diethylene glycol and mixed thoroughly. The mixture was subjected to vigorous stirring for about 30 min followed by sonication, until a clear solution was obtained. The resultant solution was subjected to

microwave irradiation at low power of 180 W. It was observed that light gray-colored precipitate was formed within a minute. On cooling, the thick precipitate obtained was centrifuged, filtered, washed and dried in hot air oven at 60 ˚C for 4-5 h. The dried product was further calcined at 500℃ for 30 min in a muffle furnace. A brown-black-colored precipitate was obtained, which was again filtered and finally dried at hot air oven at 100 ºC for 3 - 4 h.[31]

2.3.6 Green synthesis of Cu_2O nanoparticle

Green synthesis is an efficient protocol for the synthesis of various biologically active compounds with diverse molecular structures. The chemical reactions under microwave, ultrasound irradiation follows a green chemistry approach by reducing reaction time, improvement in product yield, enhancement in rate of reaction, and reducing formation of waste. This technology is environment-friendly by eliminating the use and generation of chemical hazardous and utilization of renewable raw materials.[32]

The green synthesis of nanoparticles has gained extensive attention as a reliable, sustainable, cost effective and eco-friendly protocol for synthesizing a wide range of materials/nanomaterial's including metal/metal oxides nanomaterial's, hybrid materials, and bio inspired materials. As such, green synthesis is regarded as an important tool to reduce the destructive effects associated with the traditional methods of synthesis for nanoparticles commonly utilized in laboratory and industry.[33]

Moreover, there has been a growing need to utilize indigenous resources as materials in the laboratory. The results of this study will be a basis for use of plants that are locally available in the region and in the country, as a cheaper, alternative, and important aid in chemistry.

10 ml of the tea extract was added to 10 mL of Fehling's solution and heated to 70 ºC for 5 minutes on water bath. The solution changed from blue to brick red, this indicates the formation of cuprous oxide particles. The product was now washed thoroughly with distilled water and afterwards calcined at 80 ºC.[34]

In a typical wet chemical route, at first, required amount of precursor copper sulphate ($CuSO_4$-$5H_2O$) crystals was added to double distilled water to get 1 M solution. An aqueous plant extract was made by adding about 10 g of arka leaf to 100 mL water into a conical flask and was boiled

for 1 h on a hot plate. Then, the two solutions were mixed in a proper ratio and stirred in a magnetic stirrer for half an hour at 70 °C. Under the stirring condition, hydrazine hydrate reducing agent was added drop wise till the blue color (due to Cu^{2+} ions) changed into a permanent reddish-brown suspension consisting of cuprous oxide (Cu_2O) NPs as a dispersed phase. The colloids, thus, obtained were kept standstill overnight to settle down Cu_2O NPs. After careful pouring out the upper supernatant solution, the wet solid particles were kept in an electrical oven at 80 °C for 2 h to get completely dried Cu_2O powder samples. To confirm the formation of Cu_2O NPs, 2 mL of a concentrated ammonia solution was added to 10 mg Cu_2O powders taken in a 25 mL beaker. Formation of a clear blue solution of $[Cu\ (NH_3)_4(H_2O)_2]^{2+}$ complex indicated formation of copper (I) oxide [35].

2.4 *Prunus cerasifera* (cherry plum)

Prunus cerasifera is one of the most widely grown fruit cultures in the native population of fruit species. The fruits are used mainly for the production of brandy, and the seeds are used for the production of nursery rootstock. Since Prunus cerasifera is resistable to plant diseases and pests, the chemical protection is not required. According to that, Prunus cerasifera fruits are reach and cheap source for the production of biologically healthy food. Prunus cerasifera belongs to the family Solanaceae, comprising over 2,000 species.[36]

Cherry plum might contribute to a healthful lifestyle, including: Regulates the functioning of the digestive system and thereby relieve constipation conditions due to the presence of dietary fiber, sorbitol, and isatin. Fresh plums, like yellow Mirabelle have moderate vitamin A and beta carotene content. Natural fruit's vitamin A protect from lung and oral cancer. Plums have significant amount of health promoting carotenoids such as lutein, cryptoxanthin and zeaxanthin. These compounds are one kind of scavengers against aging and disease causing oxygen-derived free radicals and reactive oxygen species. Zeaxanthin provide antioxidant and protective UV light-filtering functions. Vitamin C helps the body to develop resistance to infectious agents and scavenges harmful free radicals. Plums are rich source of potassium, fluoride and iron. Potassium as an important component of cell and body fluids, helps in controlling heart rate and blood pressure. In addition, the plums are moderate sources in vitamin B-complex groups such as niacin, vitamin B-6 and pantothenic acid and these vitamins help the body metabolize proteins, carbohydrates and fats. Plums also provide about 5 % RDA levels of vitamin K. Vitamin K is

important for clotting factors function in the blood as well as in bone metabolism and help reduce Alzheimer's disease in the elderly. Consumption of plums prevents muscular degeneration, heart diseases and also damage to our neurons and fats that form a part of our cell membranes.[37]

Prunus cerasifera are important source of compounds influencing human health and preventing the occurrence of many diseases. Plums have abundance of bioactive compounds such as phenolic acids, anthocyanin's, carotenoids, flavanols, organic acids, (e.g., citric and malic acids), fibre (pectin), tannins, aromatic substances, enzymes, minerals (e.g., potassium, phosphorus, calcium and magnesium, organic) and vitamin A, B, C & K. The predominant phenolic compounds in plums are caffeic acid, 3-O-caffeicquinic (neochlorogenic acid), 5-O-caffeicquinic (chlorogenic acid) and 4-O-caffe-icquinic (crypto-chlorogenic acid). Plums are being used in Indian medicine as a component of natural drugs used in case of leucorrhea, irregular menstruation and miscarriage. Plum helps in prevention of heart disease, lung and oral cancer, lower the blood sugar, blood pressure, Alzheimer's disease, muscular degeneration, improve memory capacity, boost bone health, regulates the functioning of the digestive system and so on. Incorporation of plums in dairy and food products like Yoghurt, Pies, Biscuits, Lassi, Ice cream etc., in form of extract, pulp, powder or dried chunks would surely boost up the nutritional and flavor quality.[38]

Anthocyanin's are the largest group of water-soluble pigments in the plant kingdom and belong to the family of compounds known as flavonoids which are part of an even larger group of compounds known as polyphenols [39]. Chemically, they are polyhydroxy and polymethoxy glycosides of anthocyanidin, derived from 2-phenylbenzopyrylium, also named flavylium cation [40].

Gallic acid and its congeners are commonly present in variety of fruits and number of plants. In addition to its natural origin, large numbers of synthesized Gallic acid derivatives are also available. It has a wide range of industrial uses including its role as standard for determing phenolic content of analytes in pharmaceutical industry, as source material for ink, paints and colour developer. Studies on Gallic acid and its derivatives have exhibited its potential for combating oxidative damages, cancer manifestations and microbial infestations. Further, Gallic acid extracted from different natural sources has been implicated to possess potency to

ameliorate neurodegenerative disorders and aging. Furthermore, large numbers of research explorations are available to show its ability for the treatment of diabetes, ischemic heart diseases, ulcer and other ailments. The structures of Gallic Acid and Some of its Derivatives are stated in Figure 2.4 and 2.5 below.[41]

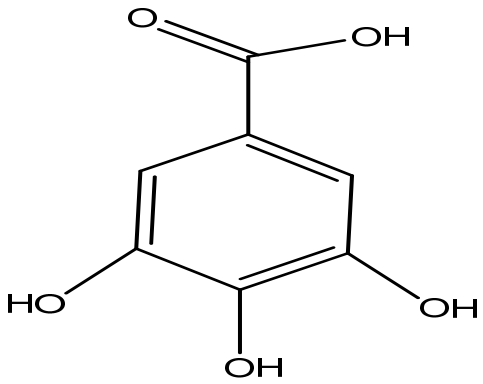

Figure Error! No text of specified style in document.**.4** General molecular structure of Gallic acid

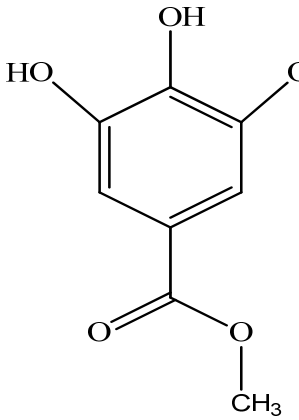

methyl gallate

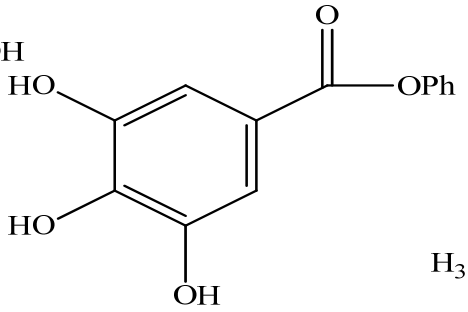

Phenyl gallate

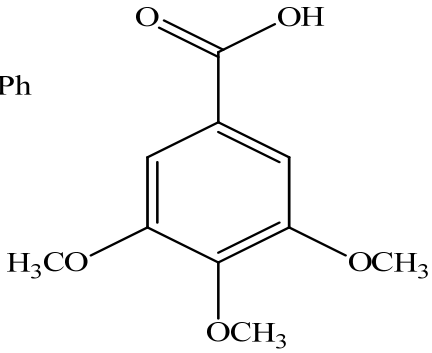

3,4,5-triacetoxygallic acid

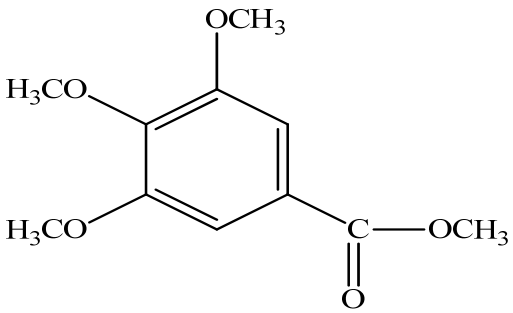

Trimethyl gallic acid methyl ester

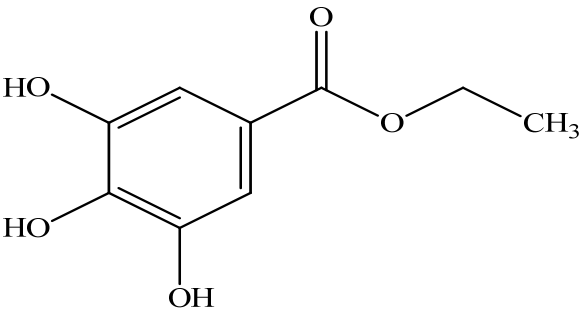

ethyl gallate

Figure Error! No text of specified style in document..**5** Derivative structures of Gallic Acid

Phenolic acids are diverse group that includes hydroxybenzoic and hydroxycinnamic acids. Various phenolic acids reported from plants are ferulic acid, ellagic acid, synergic acid, caffeic acid etc. They are also of interest in food, cosmetic and pharmaceutical industries as well as substitutes for synthetic antioxidants. One such prominent phenolic acid is Gallic acid which is found in a wide variety of vegetables, fruits, tea, coffee and wine. It occurs in plants in the form of free acids, esters, catechin derivatives and hydrolysable tannins. It also occur as methylated Gallic acids e.g., syringic acid or galloyl conjugates of catechin derivatives, i.e., flanvan-3-ols, or polygalloyl esters of glucose, quinic acid or glycerol [42]. Gallic acid has been reported to elicit various biological activities such as antibacterial, anti-fungal, antiviral, anti-inflammatory, antioxidant, anticancer, anti-diabetic etc.

Gallic acid (GA) is a phenolic compound. It is chemically known as 3, 4, 5-trihydroxybenzoic acid. The structure of Gallic acid has phenolic groups that are a source of readily available hydrogen atoms so that radicals produced can be delocalized over the phenolic structure [43].

Many Gallic acid derivatives occur naturally in plant, these include 3-O-β-D-glucopyranoside (3-glucogallic acid) and 3-O-(6- galloylglucoside), 4-O-(6-galloylglucoside) from rhubarb, mudanoside B from Paeonia suffruticosa, 3-O-dodecanoyl (3-lauroylgallic acid) with antioxidant and antimicrobial activities from Satakentia liukiuensis, 3-methyl ether from Geranium collinum and Atraphaxis frutescens, 3-methyl-5-O-sulfate (as salts) from Frankenia laevis and Tamarix amplexicaulis, 3-methyl-4-O-[3,4-dihydroxy-5-methoxybenzoyl-(6)- β-D-glucopyranoside] from Polygonum bistorta, 3-methyl-5-O-β-Dglucopyranoside from Tabernaemontana cymosa, 3-methyl ether from Poupartia axillaris and Rhus glabra, 3-ethyl ether from Phyllanthus emblica, and 4-ethyl ether from Mimosa hamata, Haematoxylum campechianum, Arbutus unedo, Eucalyptus gunnii, Terminalia chebula and Elephantorrhiza elephantine [44]. A recent study indicated presence of antioxidant Gallic acid esters (gallates) in dust from homes and microenvironments.[45]

2.5 Applications of Cu_2O nanoparticles

The major limitations of chemical method for the synthesis of Cu_2O NPs and their NCs are use of harsh and expensive chemicals, which damage the environment and are non-bio-compatible.

Nano version of Cu_2O further enhances the interest of the scientific world and motivates them to develop newer routes for its synthesis along with safeguarding the environment using least amount of harsh chemicals. In an era where every scientific activity is directly or indirectly causing great threat to the environment, a reproducible, facile, effortless, eco-friendly biological synthesis of stable and efficient Cu_2O NPs and their NCs have recently envisaged a surge in designing green protocols using both biological extracts and biological wastes (waste to wealth approach) to synthesis a wide range of NPs. Extracts from plant leaf, root, latex, seed and stem have also been used for the synthesis of NPs as they act as stabilizing/ capping agents and reducing agents both. All biological extracts have organic compounds such as polyphenols, carbohydrates, and flavones *etc.* that act as reducing agent as well as stabilizing agent. The Figure 2.6 below shows the application of CuO nanoparticles and Nano composites.[46]

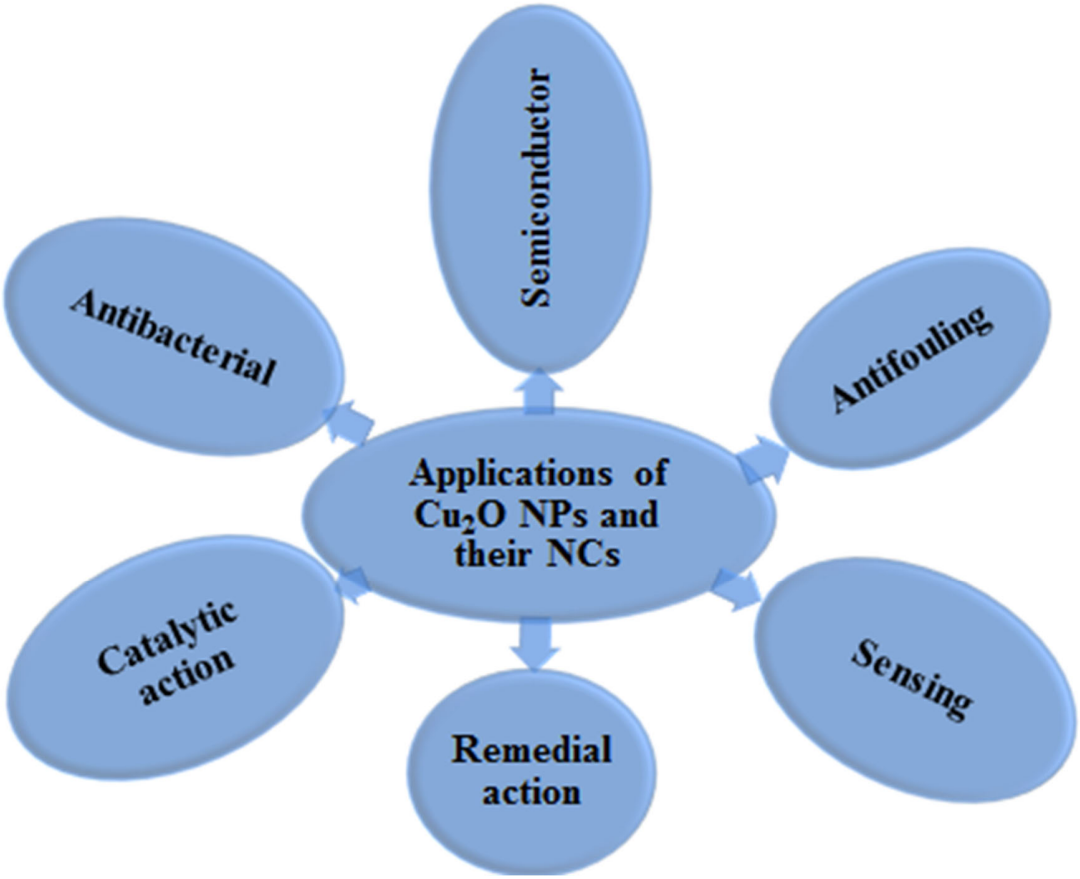

Figure Error! No text of specified style in document..**6** Flow chart showing applications of Cu_2O NPs and their NCs.

2.5.1 Hexavalent chromium [Cr(VI)] toxicity

The +6 oxidation state is of great interest because it is implicated in causing cancer in man and animals. Thus, its aqueous solution chemistry and methods for analytically determining its concentration are important. In aqueous solution, chromium(VI) may exist in a variety of Oxo species depending on pH. The structures of these anionic species are based on the sharing of a corner of the tetrahedral structure of the chromate ion as polymerization proceeds as pH is lowered. The structure of the chromate and dichromate anions where the Cr-O bond lengths are 166 pm (picometer) and 163 pm, respectively, and the bridge is 179 pm, while the Cr-O-Cr bond angle is 126º. As pH is lowered the familiar red dichromate $Cr_20_7^{-2}$ forms, followed by formation of the tri- and tetra-anions $Cr_3O_{10}^{-2}$ and $Cr_4O_{13}^{-2}$, respectively. The small size and large charge of the chromium (VI) moiety enhances its liability and engenders Cr-O double bonding (infrared stretch at 730 cm^{-1}). At pH < 1, the predominant species is H_2CrO_4, while as the pH is raised from pH 2 to 6, the $HCrO_4^-$ and $Cr_2O_7^{-2}$ anions prevail. At a pH > 8 only the yellow ion CrO_4^{-2} exists. Polymerization to the tri- and tetrachromates occurs at very low pH.[47]

Chromate salts contain the chromate anion, CrO_4^{2-}. Dichromate salts contain the dichromate anion, $Cr_2O_7^{2-}$. They are oxyanions of chromium in the 6+ oxidation state and are moderately strong oxidizing agents. In an aqueous solution, chromate and dichromate ions can be interconvertible [48].

In aqueous solution, chromate and dichromate anions exist in a chemical equilibrium.

$$2CrO_4^{2-} + 2H^+ \rightleftharpoons Cr_2O_7^{2-} + H_2O$$

Chromium is a silvery solid body-centered cubic crystal structure transition metal with atomic number 24 and atomic weight 51.9961 amu, found in group VIB, period 4 and d-block element. Hexavalent chromium is a form of the metallic element chromium. Chromium is a naturally occurring element found in rocks, animals, plants, soil, and volcanic dust and gases. It comes in several different forms, including trivalent chromium and hexavalent chromium. Trivalent chromium is often referred to as chromium (III) and is proposed to be an essential nutrient for the body. Hexavalent chromium, or chromium (VI), is generally produced by industrial processes. Chromium compounds, such as hexavalent chromium, are widely used in electroplating, stainless steel production, leather tanning, textile manufacturing, and wood preservation. The U.S. is one of the world's leading producers of chromium compounds.[49]

Hexavalent chromium exposure occurs through breathing it in, ingesting it in food or water, or direct contact with the skin. Hexavalent chromium compounds have been shown to cause lung cancer in humans when inhaled. The Report on Carcinogens lists hexavalent chromium compounds as known human carcinogens. Studies have consistently shown increased lung cancer rates in workers who were exposed to high levels of chromium in workroom air. People who work in industries that process or use chromium or chromium compounds can be exposed to higher than normal levels of chromium. Occupational exposures occur mainly among workers who handle chromate-containing pigments, spray paints, or coatings; operate chrome plating baths; or weld or cut metals that contain chromium, such as stainless steel. Some of the adverse health effects from hexavalent chromium exposures include nasal and sinus cancers, kidney and liver damage, nasal and skin irritation and ulceration, and eye irritation and damage.[49]

The presence of heavy metal ions in the aquatic environment is a great environmental concern because of their toxic properties and other adverse effects on receiving water. Among various heavy metal ions, chromium is widely used in several industrial activities such as metal processing, industrial electroplating, textiles, and plastic and leather manufacturing. The fate of chromium within the environment is closely related to its chemistry. Chromium is a heavy metal with variable oxidation states. Comparatively, hexavalent chromium (Cr(VI)) is the most toxic within the chromium species.[50]

3 MATERIALS AND METHODS

3.1 Materials

All reagents was used in this work with analytical grade and used as such without further purification. These include *Prunus cerasifera* fruit extract solution, sodium hydroxide (NaOH, 99.8%) were obtained from Alphax chemical industry, India. Dihydrated copper chloride ($CuCl_2.2H_2O$, 99%) was purchased from UNI-CHEM Chemical Reagent. Sodium chloride (NaCl, 99.8%) was obtained from Rankem Industry, India. Hydrochloric acid (HCl, 35.4%, Sp.gr. 1.18) from LOBA Chemie, India. Potassium dichromates (K2Cr2O7, 99.5%) were obtained from LOBA Chemie PVT. LTD., India. Distilled water was used throughout the whole experiment.

3.2 Identification, collection and preparation of *prunus cerasifera*

The fruit of *Prunus cerasifera* were collected from the garden of Amhara regions particularly from East Gojjam, *Sinan wereda*, 02 *kebele* of Ethiopia during the beginning of January 2020 in Ethiopia calendar as it is the blooming season of this plant for the purpose of synthesis of Cu_2O nanoparticle. The Fresh plant fruit of *prunus cerasifera* was freshly pick or cut from the end point of fruit in the morning of the day and were collected. The percentage essential phenolic acid fruit were found to be higher than that of the fresh leaves. Thus, once collected, the plant material was washed in distilled water and stored in a polyethylene bag and kept at refrigerator before use. Some amount from the stored *prunus cerasifera* fruit was chopped in to wanted pieces by spoon and juiced without adding distilled water. A 20 g of juiced *prunus cerasifera* were added to 100 mL distilled water into a conical flask and boiled for 30 minute on a hot plate. The boiled solution was cooled for 15 minute and purified. Then the mixture was centrifuged at 4000 rpm for 10 minute, to remove the insoluble (precipitate) impurities. The obtained *prunus cerasifera* extract solutions were kept at refrigerator for further experiments. The flow chart below in Fig. 3.1 was used to prepare *Prunus cerasifera* fruit extract solution. And also *prunus cerasifera* was identified taxonomically in Department of Biology by Mesfin Woldearegay (Ph.D), plant biology and biodiversity management, Debre Berhan University.

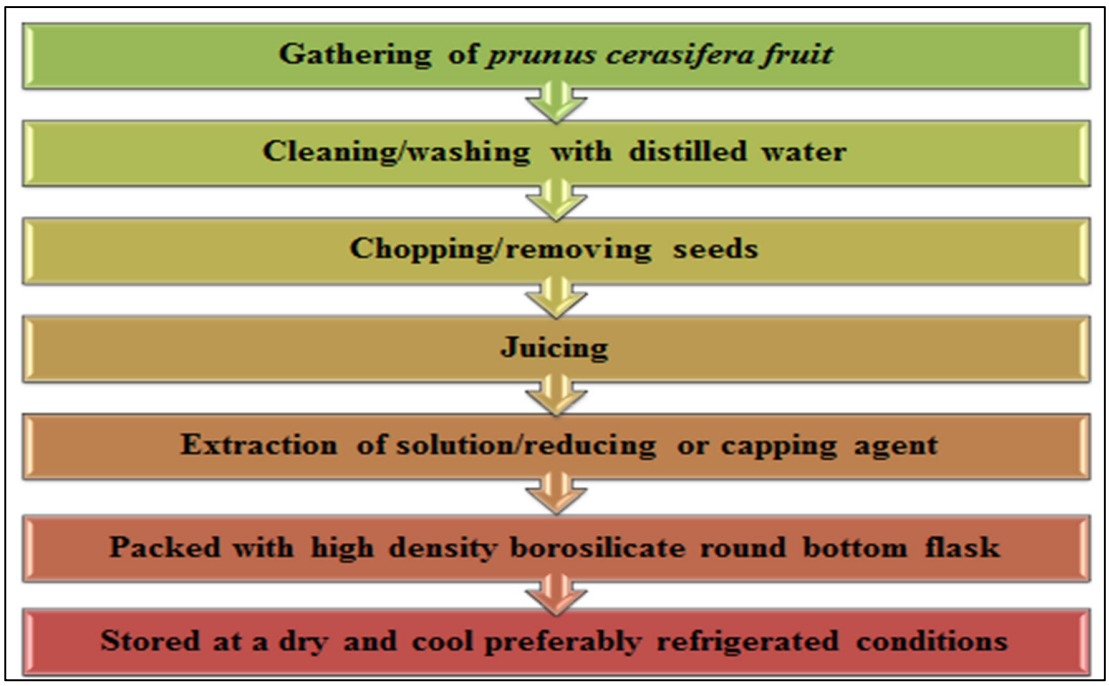

Figure Error! No text of specified style in document..**7** Production of *prunus cerasifera* fruit extracts solution flow chart

Figure 3.2 below shows the photographic picture of fruit, juice and solution samples of the *prunus cerasifera* plant.

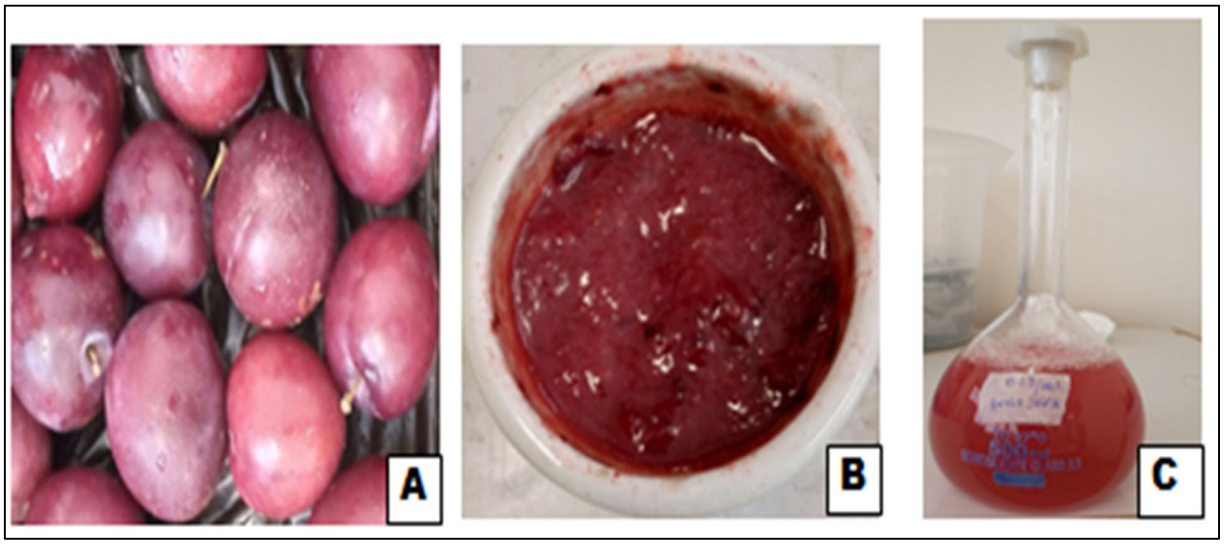

Figure Error! No text of specified style in document..**8** Photographic pictures of *prunus cerasifera* (A) fruit **(**B**)** juice (C) extract solution

3.3 Synthesis of the Cu_2O nanoparticle

In a typical green synthesis method, a 100 mL of 0.2 M $CuCl_2 \cdot 2H_2O$ solution and 50 mL of 0.2 g/mL *prunus cerasifera* fruit juice extract solution (Gallic acid, $C_6H_2(OH)_3COOH$) properly and gently mixed together by a heating magnetic stirrer for 15 minute followed by a drop wise addition of a 15 mL of NaOH (3M) gradually for 40 minute to the mixture under vigorous stirring till light blue color (due to Cu^{2+} ions) changed into a permanent brick- red suspension consisting of cuprous oxide (Cu_2O) nanoparticle as a dispersed phase. The mixture stirred at 80 ˚C for 5 hour**.** The colloids, thus, obtained were washed with distilled water three times and kept standstill overnight to settle down Cu_2O NPs. After careful pouring out the upper supernatant solution, the wet solid particles were kept in an electrical drying hot air oven at 110 °C for 2 h to get completely dried Cu_2O powder samples. The flow chart in Fig. 3.3 below was used to synthesize, characterize Cu_2O nanoparticle and how it had been applied for the photocatalytic reduction of hexavalent chromium [Cr (VI)].

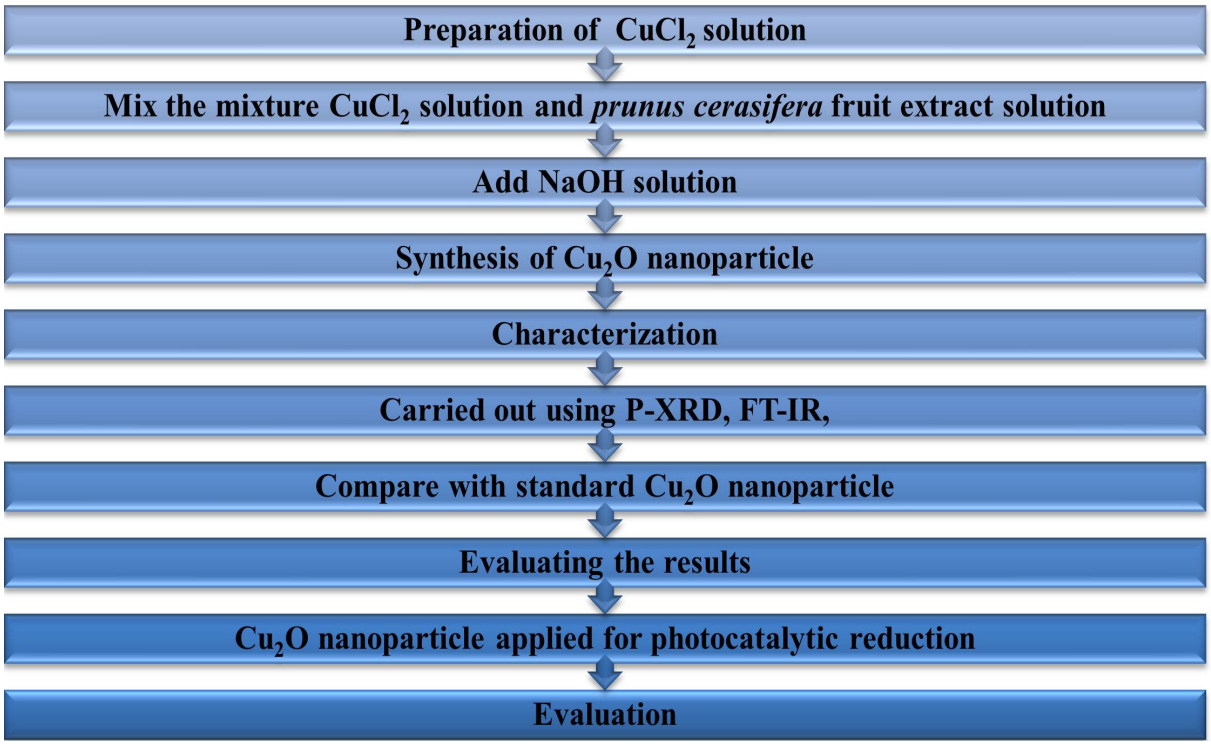

Figure Error! No text of specified style in document.**.9** Flow chart of the synthesis, characterization and catalytic application of Cu_2O nanoparticle

3.4 Characterization of Cu_2O nanoparticle

3.4.1 X-Ray Diffraction

Powder X-Ray diffraction technique is a powerful technique to analyze the crystalline and amorphous nature of the material under investigation. In crystalline materials, peaks were observed whereas in amorphous material show broad peaks instead of sharp peaks.

X-ray diffraction of Cu_2O nanoparticle was performed on advance X-ray diffractometer (SHIMADZU, XRD-7000 X-RAY DIFFRACTOMETER) using 40 kV and 45 mA, with a Cu-Kα (λ = 1.54056 Å) radiation. Normal XRD scans with step resolution of 0.02 degrees (2θ) with a time step of 0.3s were used. The Cu-Kα2 diffraction signal was removed by a standard stripping procedure to obtain the correct lattice parameters and particle size.

3.4.2 Fourier Transform Infrared Spectroscopy

The surficial functional groups of the pure Cu_2O, and Cu_2O/*Prunus cerasifera* were characterized by a Fourier transform infrared (FT-IR) spectrophotometer.

The Fourier transform infrared spectra of Cu_2O/Prunus cerasifera nanoparticle were recorded using Perkin Elmer FT-IR (spectrum Two, CE/QE/IR-02/113) spectrometer in the range 450-4000 cm^{-1}. Analysis of these vibrational absorption bands provides information about the chemical species present. This includes information about the structure of Cu_2O as well as other functional group.

3.4.3 Point of zero charge

The pH of point of zero charge of Cu2O nanoparticle was determined to know the surface charge of cuprous oxide nanoparticles. For this purpose, 30 mL of sodium chloride (0.01M, NaCl) solution was placed in a100 mL Erlenmeyer flask.

The pH of the suspension at which the net zero charges on the surface of the insoluble oxide/hydroxide to play an important role in characterization of metal oxide/hydroxide was determined by the point of zero charge (PZC). To examine the point of zero charge, the pH was then adjusted to successive initial pH values (2, 4, 6, 8, and 10) by using either sodium hydroxide or hydrogen chloride (0.1 M). A 0.03g of Cu_2O nanoparticle catalyst was added to 30 mL of initial concentration for a contact time of 24 hrs. After the rotary shaking a contact time of 24 hr.

the final pH was measured and ΔpH was calculated and it plotted against the initial pH. The pH at which the curve crosses the line pH (final - initial) is taken as optimum pH or pH of point of zero charge (pH_{PZC}).

3.5 Photocatalytic reduction study of Cr (VI)

The maximal wavelength absorption of hexavalent chromium [Cr(VI)] solution were recorded using UV/Vis spectrophotometer (AE1408013) and scanning in the specific wavelength range of 340 nm to 380 nm. The small amount of hexavalent chromium solution was measured and placed in the quartz cuvette. The wavelength of maximum absorption of the hexavalent chromium solution was selected and it is used to determine the absorbance of Cr (VI) solution in different concentration (10 mg/L, 30 mg/L, and 50 mg/L) at 0, 30, 60, 90, 120, 150, and 180 min. The value of absorbance at each time (min) was determined and the photocatalytic reduction of hexavalent chromium was interpreted.

The Cu_2O nanoparticle was applied for the photocatalytic reduction of the toxic or carcinogenic hexavalent chromium [Cr (VI)]. The estimated weight of photocatalyst was introduced into the hexavalent chromium solution. Nanophoto-catalysts assisted chromium solution was exposed to solar irradiation for different time periods. The spectrum was recorded for every time interval using UV-visible absorption spectrophotometer at constant chromium (VI) concentration and dose level, for various irradiations time periods. From the recorded spectra, the percentage of chromium (VI) removal was calculated using the standard formula.

The stock solution of hexavalent chromium [Cr (VI)] of concentration 50 mg/L was prepared by dissolving (0.071 g) of $K_2Cr_2O_7$ in 500 mL volumetric flask, agitated by using a magnetic stirrer. Reduction expresses the quantity of material reduced per unit mass of adsorbent as a function of the equilibrium concentration of the adsorbate. The reduction process was investigated as a function of solution pH, contact time, adsorbent dose and adsorbate dose. The pH of the solution was adjusted to the required value by adding 0.1 M HCl or 0.1 M NaOH. The necessary data were derived from experiments where a specified mass of adsorbent is equilibrated with a known volume at a specific concentration of a chemical and measured in solution by the mass balance equation [49].

$$\% \text{ Reduction} = \frac{A_o - A_t}{A_o} * 100 \quad \text{..... (3)}$$

Where A_0 is the initial absorbance of a solution and at is the absorbance of a solution after a process of reduction in at period of time "t".

3.5.1 Effect of pH on Hexavalent Chromium

To examine the effect of pH on hexavalent chromium, the pH of a solution was adjusted to different value ranges between 4 and 9. A fixed amount of the Cu_2O catalyst, 0.03g was added to 30 mL of initial concentration for a contact time varying between 30 and 180 min. After the reduction time was completed the pH with the highest reduction efficiency was taken as the optimum pH.

3.5.2 Effect of Contact Time

The effect of contact time of the Cu_2O nanoparticle catalyst with Cr(VI) solution was studied by measuring the hexavalent chromium absorbance. The experiment was conducted at different contact times (30, 60, 90,120, 150, 180 min) using 10 mg/L,30 mg/L and 50 mg/L of hexavalent chromium [Cr(VI)] and by addition of 0.03g of Cu_2O nanoparticle catalyst and calculated the % reduction.

3.5.3 Effect of Adsorbent Dosage on the Adsorbate

The reduction of hexavalent chromium by synthesized Cu_2O nanoparticle catalyst was investigated using the adsorbent dose of 20, 40, 60 and 80 mg in 10 mg/L of adsorbate concentration at 0 and 30 min determine the maximum reduction efficiency.

3.5.4 RSM-BBD optimization of photocatalytic reduction variables

The photocatalytic reduction of Cr(VI) was carried out in a batch reactor at different concentrations of Cr(VI). Specifically, 30 mg of the Cu_2O catalyst was added to 30 mL of Cr(VI) solution (10-50 mg/L) and stirred continuously. After adding the reduction catalyst, the initial (time $t = 0$) for the reaction. The pH of the solution was adjusted using NaOH (0.1 M) and HCl (0.1 M). The reduction (%) of Cr(VI) was analyzed by measuring the absorbance at λ = 350, 358,365 nm using an ultraviolet-visible spectroscopy. The RSM-BBD optimization of Cr(VI) reduction mainly focused on 3 independent variables: pH, contact time (minutes), and concentration of Cr(VI) in mg/L. These 3 variables are selected because catalysis processes are

highly dependent on them. The other remaining variables including 30 mg of catalyst dose in 30 mL solution (0.03 mg/mL), and room temperature (298 K) were fixed throughout the whole reaction process. Design Expert 11 software program was used to compute the statistical analysis. The experimental levels of factors used for RSM-BBD are given below in table 3.1.

Table Error! No text of specified style in document.**.2**. The experimental levels of factors used for RSM-BBD.

Factor	Name	Unit	Level		
			Low (-1.000)	Medium (0.000)	High (1.000)
A	pH		4	6.5	9
B	Contact time	Min	30	105	180
C	Cr(VI) concentration	mg/L	10	30	50

3.5.5 Reduction Kinetics

First order kinetics:

The kinetics of Cr(VI) reduction can be studied by evaluating the decreasing in absorbance at 365 nm wavelength using UV-Vis spectroscopy , visible/cuprous oxide catalyst (80 mg) and 30 mL of 10 ppm Cr(VI). The first order model for reduction kinetics data which is the earliest known equation describing the reduction rate based on the reduction efficiency [51, 52]. The differential equation is generally express as follows.

$$-\frac{d[Cr(VI)]}{dt} = k_1[Cr(VI)] \quad \text{.....(4)}$$

Where: Cr(VI) is the concentration of hexavalent chromium, k_1 is the rate constant of first order reduction (min^{-1}) and t is the contact time (min).

Integrating equation (4) for boundary conditions (t = 0, [Cr(VI)] = C_o and t = t, [Cr(VI)] = C_t) leads to the following linear equation:

$$\ln\frac{C_o}{C_t} = k_1 t \quad \text{.....(5)}$$

The linearized integral form of the first order kinetic model is generally expressed as follows.

$$\log C_t = \log C_o - (k_1/2.303)*t \quad \text{..... (6)}$$

To plot $\ln\frac{C_o}{C_t}$ or versus t give a linear relationship from which k_1 can be determined from the slope of the plot.

Equation (5) can be rearranged in a nonlinearized form: $C_t = C_o * e^{-(k_1*t)}$ .....(7)

4 RESULTS AND DISCUSSION

4.1 Synthesis of Cu_2O nanoparticle

The synthesis of cuprous oxide nanoparticles by the green synthesis is based on dihydrated copper chloride ($CuCl_2.2H_2O$) as a starting material or precursor. The followed mechanism is proposed to explain the formation of the Cu_2O nanoparticles. The hydrolysis reaction:

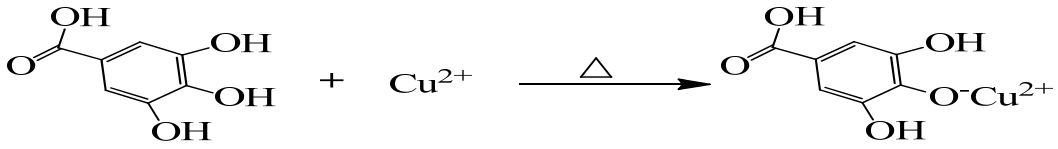

…….. (1)

This complex is then transformed into $Cu(OH)_2$ by the addition of NaOH. The condensation process is initiated by NaOH addition:

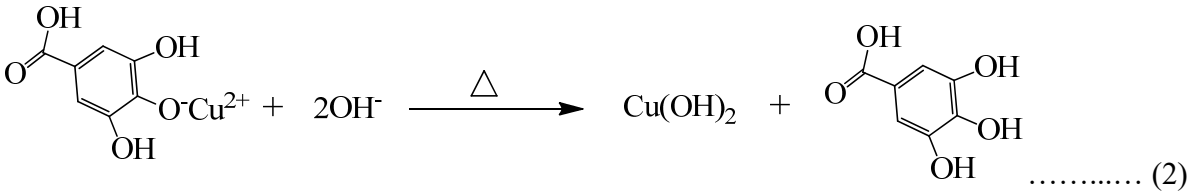

……..… (2)

After 40 minute gradual addition of OH^-, the Cu_2O is formed by oxidation of Gallic acid, GA

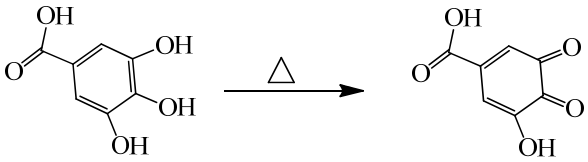

.....(3)

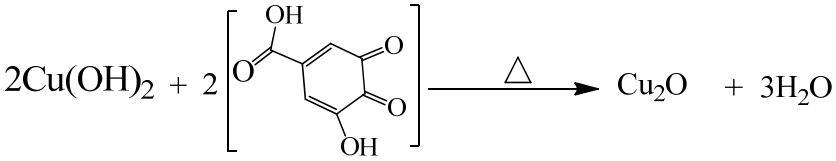

..... (4)

According to these equations, Gallic acid (GA) and sodium hydroxide are the two key factors which orient the synthesis of Cu_2O nanostructures by controlling the pH medium (pH = 10).

Fig. 4.1 below resumes the solution color variation which indicates the modification of copper-based chemical species present in the solution as a function of pH.

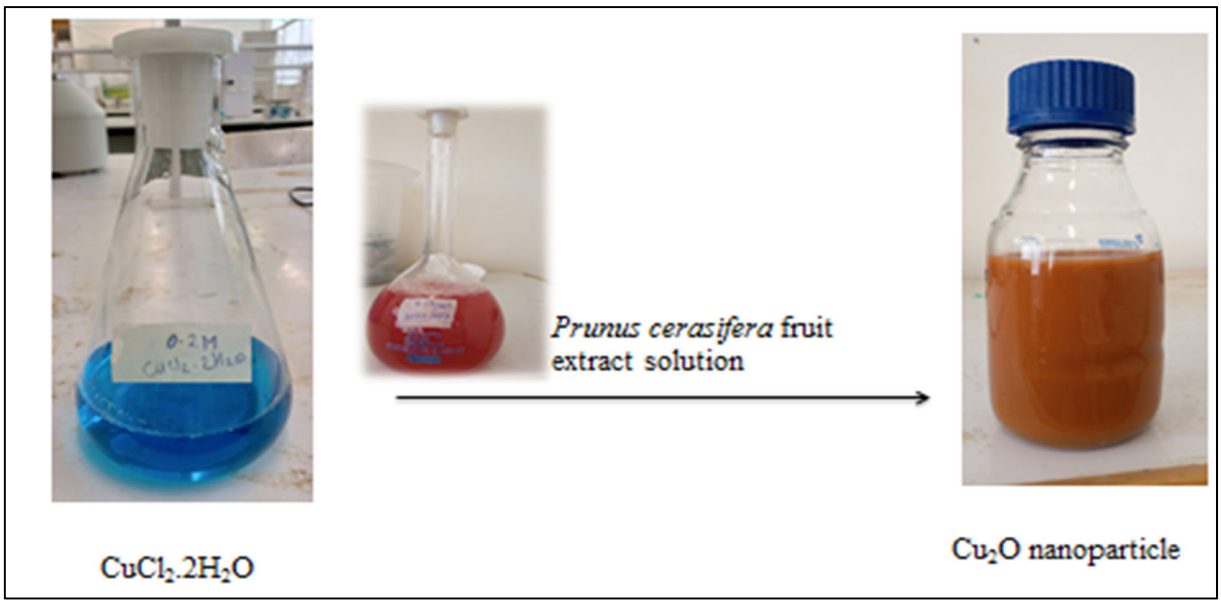

Figure Error! No text of specified style in document..**10** Schematic illustration of color change in the synthesis of Cu_2O nanoparticles coated with *prunus cerasifera*

4.2 Characterization

4.2.1 X-Ray Diffraction Analysis

Figure 4.2 shows the XRD pattern of Cu_2O nanoparticles sample, which is prepared by green synthesis via precipitation method and clearly reveals the structure of crystalline. The peaks in this pattern are sharp and have no significant scattering background.

The most important change observed in the XRD pattern is the appearance of the characteristic peaks of Cu_2O nanoparticles sample. Based on the XRD pattern shown in the Figure 4.2 (b) below, Cu_2O exhibits a phase having a cell parameter of 4.256 Å and space group Pm-3m (224). This cubic phase of Cu_2O phase is as per the standard XRD. By taking strongest 3 peaks the average crystallite size is 32.717 nm, which is measured by Scherer's equation. And all the peaks match well with standard data (COD CIF, No. 00-100- 0063). The crystallographic planes in a crystal (111) peak at 36.5656 (d = 2.45547) is the most strong peak of the pattern, and (110) peak at 39.7540 (d=2.26557) is the weakest in intensity. The Figure 4.2 indicated the synthesized Cu_2O nanoparticles product obtained by using 20% (w/v) concentration *prunus cerasifera* extract solution shows most similar peaks with standard cuprous oxide (Cu_2O) data than 10% (w/v) extract solution . The XRD shows the final product is a Cu_2O sample.

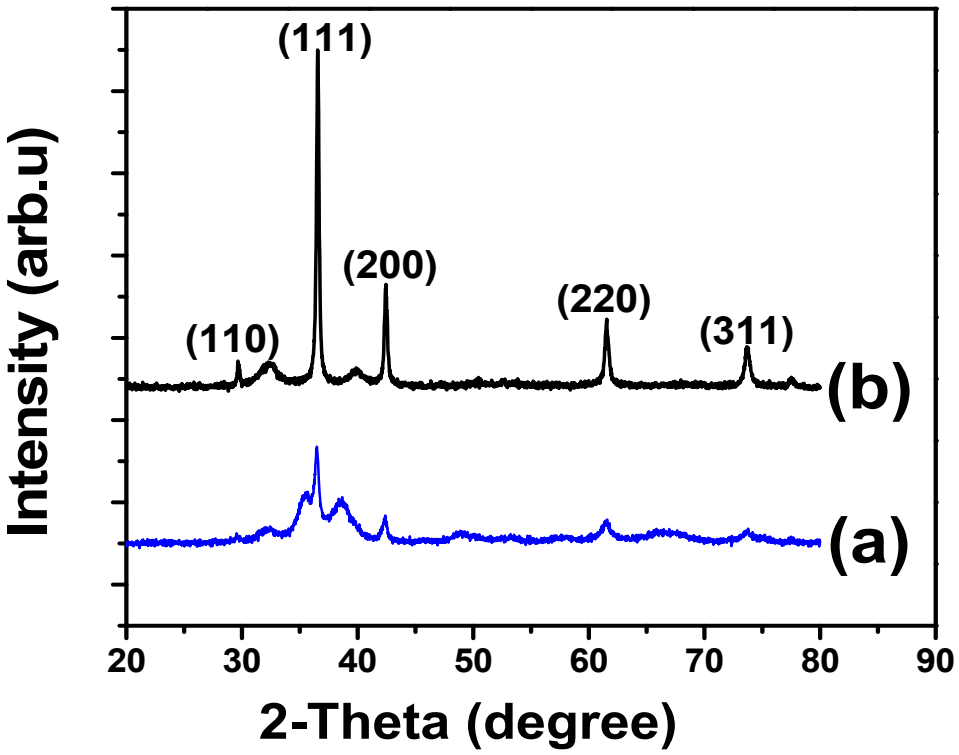

Figure Error! No text of specified style in document..**11** XRD patterns of Cu_2O nanoparticles sample that synthesized with (a) 10% (b) 20% (w/v) *prunus cerasifera* extract solution.

4.2.2 Fourier Transform Infrared Spectroscopy Analysis

The Fourier transform infrared spectroscopy was used to investigate the vibrational functional group present in the *Prunus cerasifera* fruit extract solution and Cu_2O nanoparticle. The FT-IR spectra of *Prunus cerasifera* solution indicated in the Figure 4.3, the characterization peak 1450 - 1600 cm^{-1} was due to C=C, 1000-1300 cm^{-1} was due to C-C and 1650-1725 cm^{-1} for C=O vibrational bands in the solution. The vibrational bands at 3000-3600 $cm^{-1}$was due to the presence of C-H and O-Hs bond stretching.

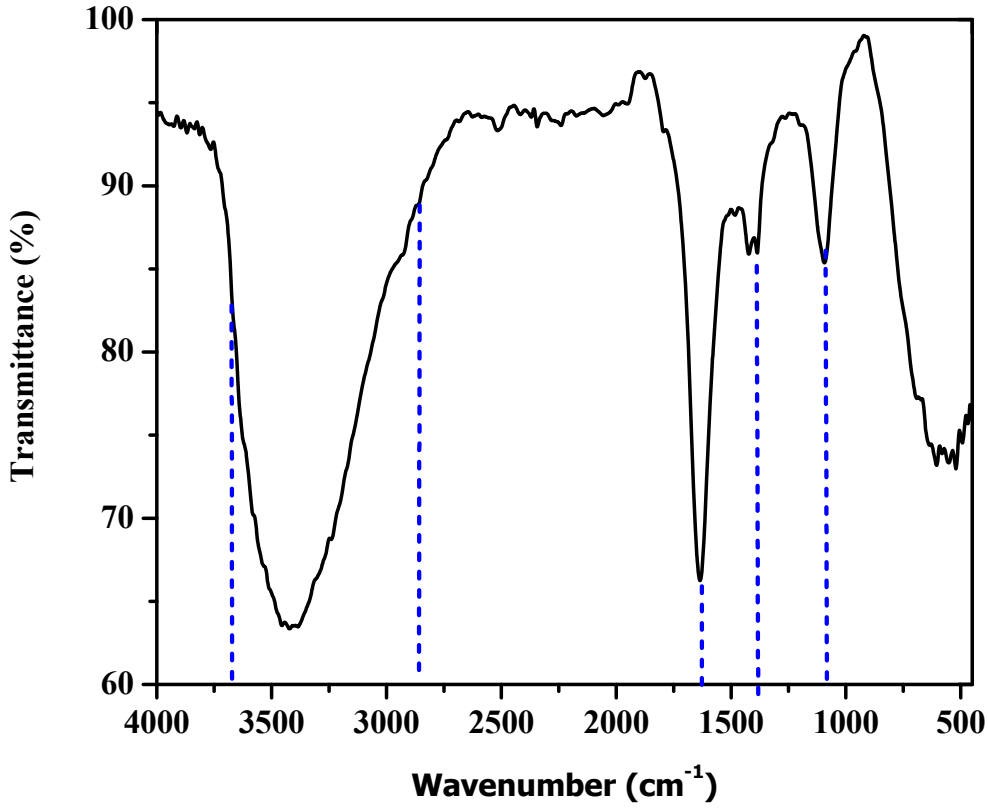

Figure Error! No text of specified style in document.**.12** The FT-IR spectra of *prunus cerasifera* fruit extract solution

The FT-IR spectra of Cu_2O nanoparticle sample indicated in Figure 4.4 below, the vibrational bands at 3400 cm^{-1}, was due to O-H stretching in the treated on concentration of those sample. The FT-IR characteristic peaks of the vibration observed at the region of 625 cm^{-1} in the control of sample was due to Cu-O stretching vibration, which is in good agreement with literature values [53, 54]. The vibrational bands at 1115, 1620, 1630, cm^{-1} was due to C-C, C=C and C=O vibrational bands respectively in the sample and 1400 cm^{-1} due to C-H and O-H bending peaks.

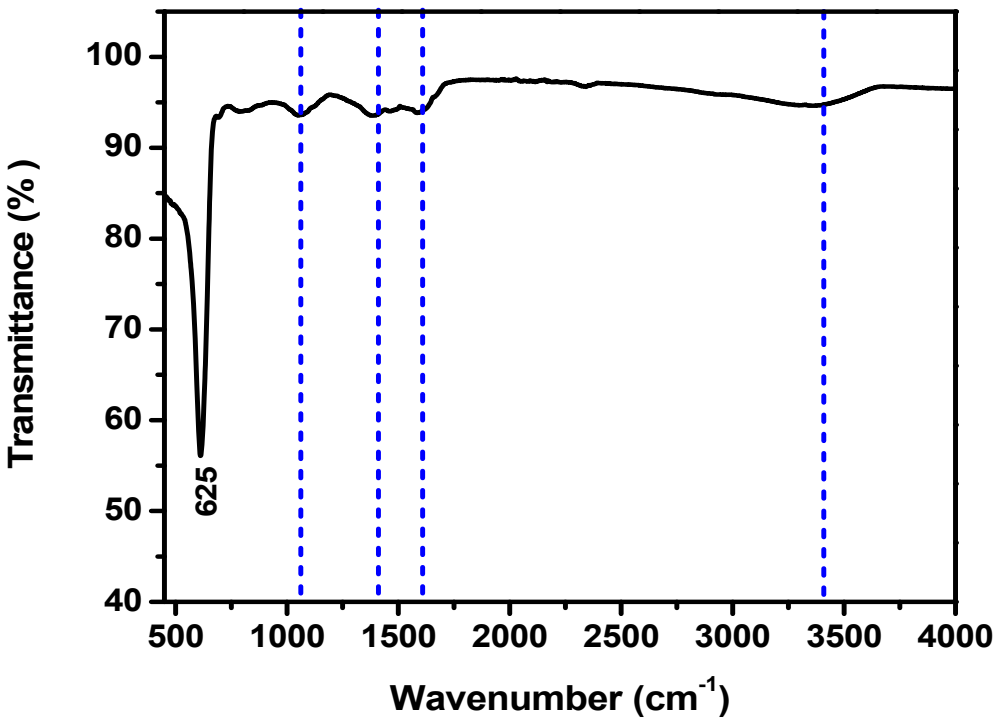

Figure Error! No text of specified style in document.**.13** FT-IR spectra of Cu_2O nanoparticle sample

4.2.3 Point of zero charge

Zeta potential is a possible method for determining the point of zero charge of a nanoparticle. In an ionic solution, nanoparticles with a net charge will have a layer of ions (of opposite charge) strongly bound to their surface; this is referred to as the Stern layer. A second diffuse outer layer is comprised of loosely associated ions. These two layers are collectively called the electrical double layer. As the particle moves (due to Brownian diffusion or applied force), a distinction is created between ions in the diffuse layer that move with the nanoparticle and ions that remain with the bulk dispersant. The electrostatic potential at this "slipping plane" boundary is called the zeta potential and is related to the surface charge of the nanoparticle.[55]

The measurement of the electrostatic potential at the electrical double layer surrounding a nanoparticle in solution. Nanoparticles with a zeta potential between -10 and +10 mV are considered approximately neutral, while nanoparticles with zeta potentials of greater than +30 mV or less than -30 mV are considered strongly cationic and strongly anionic, respectively.

Since most cellular membranes are negatively charged, zeta potential can affect a nanoparticle's tendency to permeate membranes, with cationic particles generally displaying more toxicity associated with cell wall disruption.[56]

The pH of point of zero charge of the Cu_2O was determined. The pH_{PZC} is the pH at which the Cu_2O has a neutral charge on the surface. The pH_{PZC} for the Cu_2O was found to be 6.9 at which the curve crosses the line pH (final - initial). If pH of the solution is less than pH_{PZC}, the adsorbent surface becomes negative and attracts cations from the solution, and if pH of the solution is greater than pH_{PZC}, the surface becomes positive and attracts anions from the solution. The point of zero charge is a fundamental description of a mineral surface and is more or less the point where the total concentration of surface anionic sites is equal to the total concentration of surface cationic sites.

As shown in Figure 4.5 below at a pH < 6.9 the Cu_2O surface has a negative charge and adsorbs the cationic chromium via electrostatic attraction. Under these conditions, the attraction between hexavalent chromium cations and the adsorbent surface, and the subsequent high adsorption may expect.

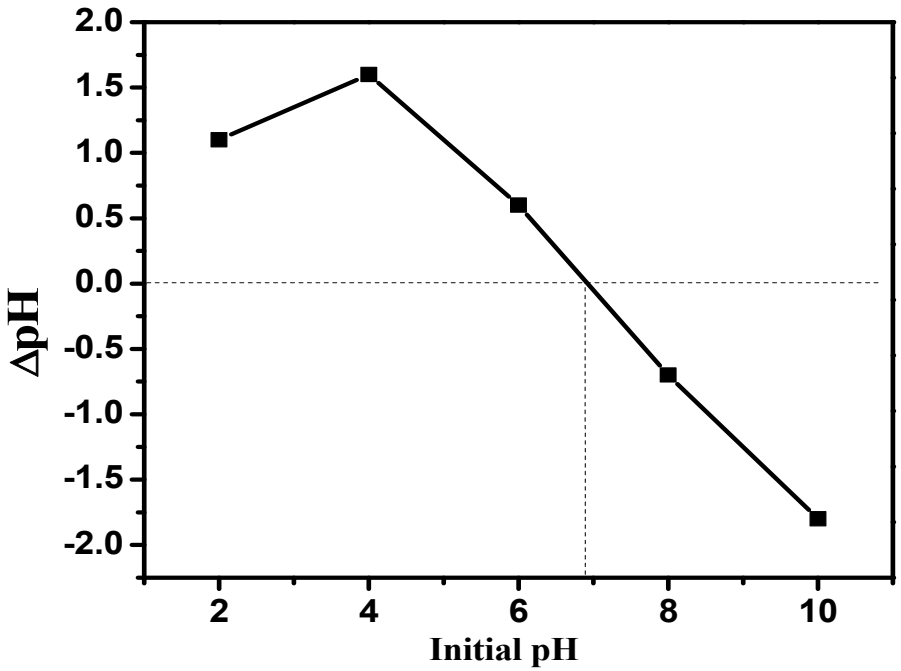

Figure Error! No text of specified style in document..**14** The pH of point of Zero charge of Cu_2O obtained from green synthesis.

4.3 Photocatalytic reduction study of Cr(VI)

The maximum absorbance wavelength of 10 mg/L, 30 mg/L, and 50 mg/L Cr(VI) absorption lays at 365, 358 and 350 nm respectively, under the acidic conditions. The observed maximal absorption wavelength of 350, 358 and 365 nm is comparable to other literature data value. The Cr(VI) reduction absorbance was analyzed by UV/vis spectrophotometer. The detailed Cu_2O/visible light reduction of Cr(VI) UV-Vis spectrophotometer analysis was stated.

The white fluorescent visible lamp (model: ultra violet cabinet) with approximately 15 watts maximum output was used as a visible light source and located within the inner tube. After the pre-warmed light source was turned on, aliquots of the reaction solution was withdrawn at intermittent periods of reaction time. The aqueous samples were filtered by an 800D centrifuge machine at 3000 rpm to remove Cu_2O particles within 5 min and subsequently analyzed for Cr(VI) and total Cr.

4.3.1 Effect of pH and contact time

As shown in Figure 4.6 below, effect of pH and contact time on the reduction efficiency of Cu_2O nanoparticle. The sample of hexavalent chromium was taken in separate beakers and reduction studies were carried out at different pH and different contact time with a fixed dose of adsorbent (0.04 gm.).

The effect of the pH on the reduction of hexavalent chromium on Cu_2O adsorbent catalyst was investigated at initial pH value varying between 4.0 and 9.0. The effects of initial pH on reduction were obtained maximum at low pH value. The reduction of these positively charged Cr(VI) groups on the adsorbent surface was primarily influenced by the surface charge on the adsorbent which in turn is influenced by the solution pH. The result showed that the availability of negatively charged groups at the adsorbent surface was necessary for the reduction of toxic hexavalent chromium. Thus, as the pH decreased, more negatively charged surface was available for greater reduction of Cr(VI) .

The effect of contact time on the reduction of hexavalent chromium on Cu_2O adsorbent catalyst was investigated at a specific time value varying between 30 and 180 min. In the present investigation, it was observed that as the contact time increase the reduction efficiency was increase.

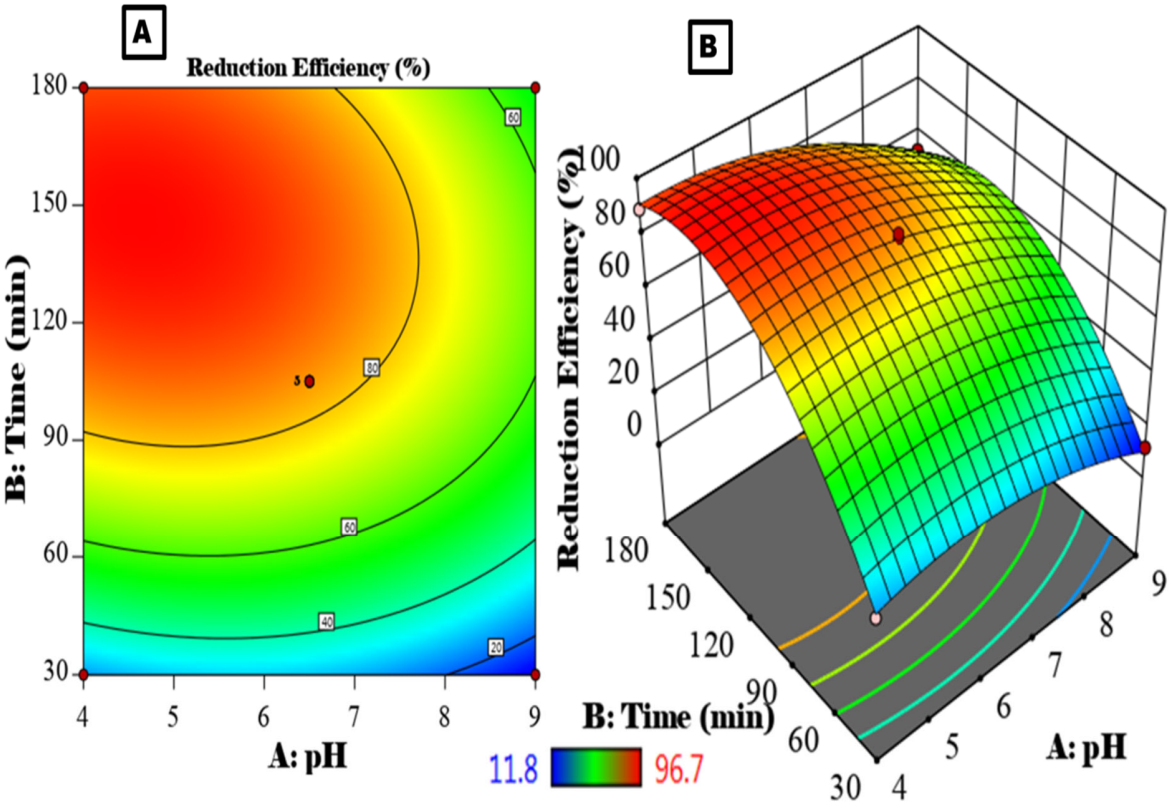

Figure Error! No text of specified style in document.**.15** Effect of pH and contact time on reduction efficiency (A) 2D and (B) 3D surface plot

4.3.2 Effect of pH and Cr(VI) concentration

Figure 4.7, shows the effect of pH and concentration of Cr (VI) on the reduction efficiency of Cu_2O. The sample of hexavalent chromium [Cr(VI)] was taken in separate 80 mL beakers and reduction studies was carried out at different pH (4, 6.5 and 9) and different concentration of Cr(VI) (10 mg/L,30 mg/L and 50 mg/L) with a fixed dose of adsorbent (0.04 gm.). In the present investigation, it was observed that as the pH and Cr(VI) concentration decrease the reduction efficiency was increase.

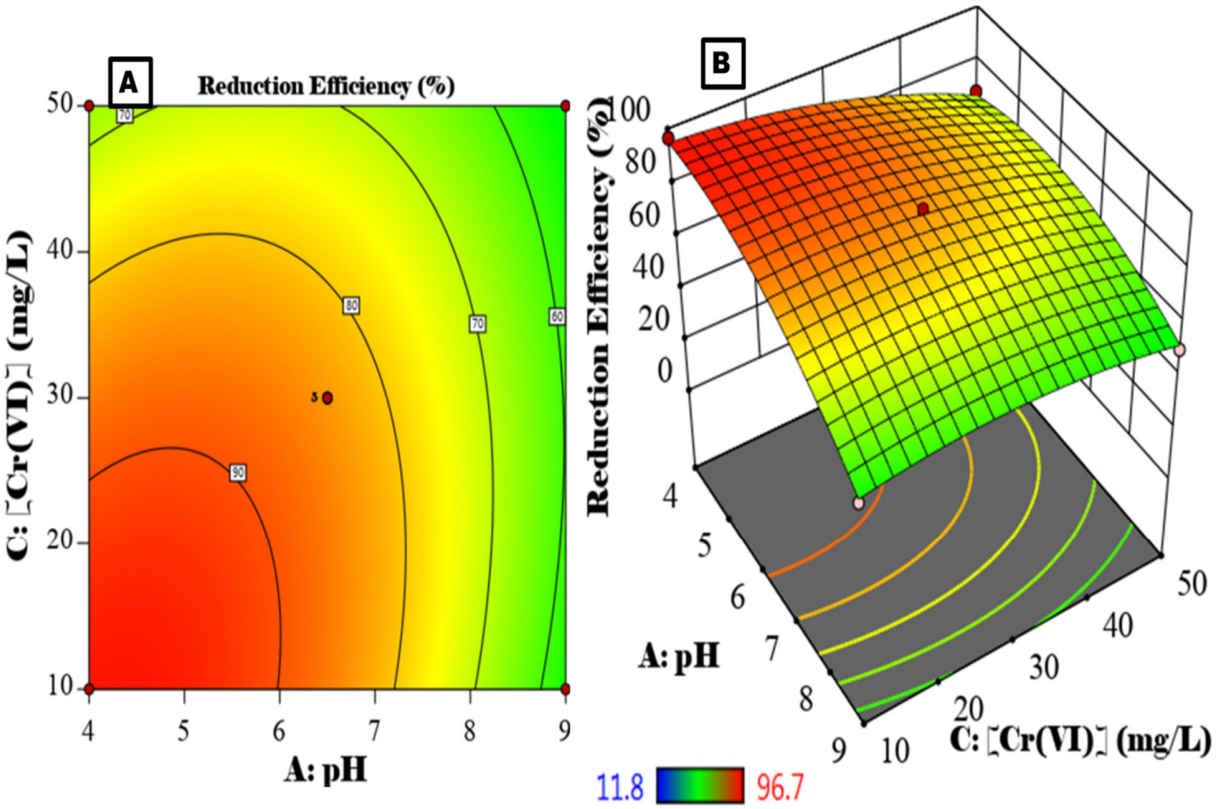

Figure Error! No text of specified style in document..**16** Effect of pH and Cr(VI) concentration (A) 2D (B) 3D surface plot

4.3.3 Effect of contact time and Cr(VI) concentration

The effect of contact time and concentration of Cr (VI) on the reduction efficiency of Cu_2O. The sample of hexavalent chromium was taken in separate 80 mL beakers and reduction studies was carried out at different contact time (30 min, 105 min and 180 min) and different concentration of hexavalent chromium (10 mg/L, 30 mg/L and 50 mg/L) with a fixed dose of adsorbent (0.04 gm.).

As shown in the Figure 4.8 below, the present study was observed that as the contact time increase the reduction efficiency was increase and vice versa for concentration.

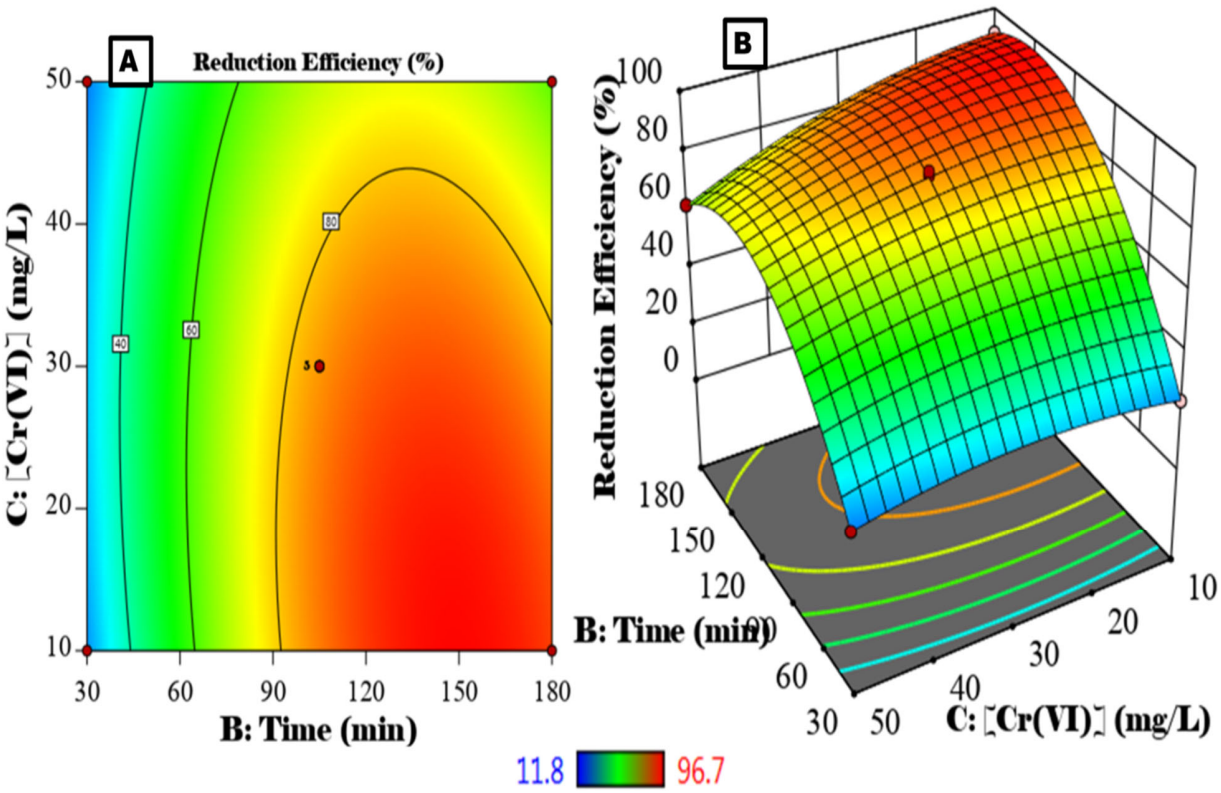

Figure Error! No text of specified style in document.**.17** Effect of contact time and Cr(VI) concentration (A) 2D (B) 3D surface plot

4.3.4 Effect of Cu_2O sample dose

The effect of adsorbent (Cu_2O nanoparticle) dose towards Cr(VI) was investigated. A 20 mL and fixed concentration of 10 mg/L Cr(VI) as a function of dosage of Cu_2O sample powder of (0.02, 0.04, 0.06 and 0.08 gm.).The pH was adjusted to be 3. The maximum absorbance wavelength of 10 ppm Cr(VI) absorption lays at 365 nm. After one hour the absorbance of Cr(VI) were recorded by using UV-Vis spectrophotometer. It was found that by increasing the adsorbent dose the percent of reduction efficiency also increase. As shown in the Figure 4.9 the reduction efficiency of Cu_2O was found to be 82.9 , 88.05 , 91.9 and 95.1% at the end of one hour for 0.02, 0.04, 0.06 and 0.08 gm. respectively. Therefore, Cu_2O catalyst material has a great capacity for reduction efficiency of hexavalent chromium.

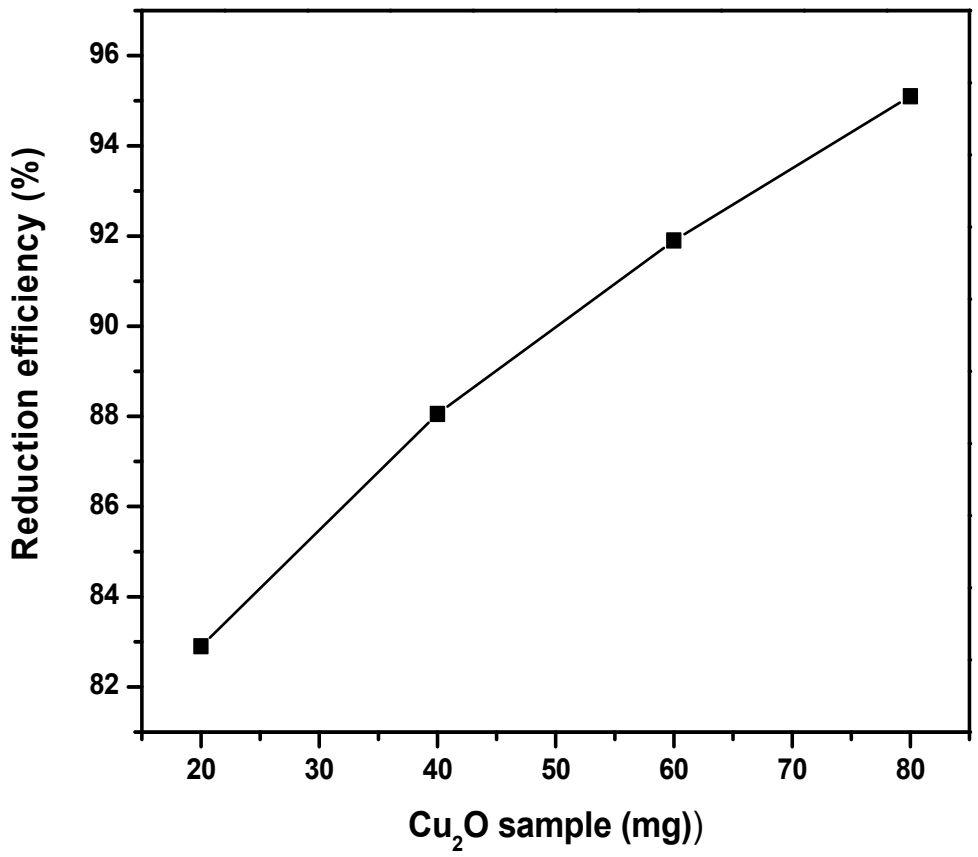

Figure Error! No text of specified style in document..**18** Effect of Cu_2O nanoparticle sample dose on Cr(VI)

4.3.5 Optimization of Cr(VI) reduction using RSM-BBD

During photocatalysis reaction, optimizations of the process variables using statistical approaches are crucial for the economic utilization of time and resources. Moreover, the statistical analysis gives a clear understanding of the reaction process and minimizes the experimental errors. Herein, the RSM-BBD approach was applied to optimize the photocatalytic reduction of Cr(VI) using Cu_2O nanoparticle. The complete BBD matrix for the 3 independent variables (pH (A), contact time (B), and Cr(VI) concentration (C)) and the response of both coded and real values are presented in Table 4.1.

Table Error! No text of specified style in document..**3.** The RSM-BBD design matrix of the 3 variables with coded and real values, and response with actual and predicted values.

Run order	Coded values			Real values			Response	
	A	B	C	A	B	C	Actual	Predicted
1	1.000	0.000	1.000	9	105	50	50.50	52.20
2	0.000	0.000	0.000	6.5	105	30	82.40	84.04
3	-1.000	1.000	0.000	4	180	30	89.10	90.74
4	0.000	1.000	1.000	6.5	180	50	62.00	61.74
5	0.000	-1.000	-1.000	6.5	30	10	23.70	23.96
6	0.000	0.000	0.000	6.5	105	30	84.60	84.04
7	-1.000	-1.000	0.000	4	30	30	23.50	24.94
8	-1.000	0.000	-1.000	4	105	10	96.70	95.00
9	0.000	0.000	0.000	6.5	105	30	86.00	84.04
10	1.000	0.000	-1.000	9	105	10	54.40	55.77
11	0.000	-1.000	1.000	6.5	30	50	21.90	21.84
12	0.000	0.000	0.000	6.5	105	30	83.20	84.04
13	0.000	1.000	-1.000	6.5	180	10	91.50	91.56
14	1.000	-1.000	0.000	9	30	30	11.80	10.16
15	-1.000	0.000	1.000	4	105	50	68.00	66.62
16	0.000	0.000	0.000	6.5	105	30	84.00	84.04
17	1.000	1.000	0.000	9	180	30	53.30	51.86

The empirical relationship between experimental parameters and % reduction efficiency was expressed as it is shown in equation 8 below [57]:

$$Y = b_o + \sum_{i=1}^{n} b_i X_i + \sum_{i=1}^{n} b_{ii} X_i^2 \sum_{i=1}^{n-1} \sum_{j=i+1}^{n} b_{ij} X_i X_j \quad \ldots\ldots\ldots\ldots\ldots\ldots\ldots\ldots\ldots\ldots\ldots\ldots\ldots\ldots\ldots\ldots\ldots\ldots\ldots\ldots\ldots\ldots (8)$$

Where Y is the predicted response (reduction, %) of Cr(VI); b is a constant ; and b_o, b_i, b_{ii} and b_{ij} are the regression coefficients for the intercept, linear, quadratic, and interaction coefficients, respectively. X_i and X_j are independent variables from the lists of the coded values of factors and n=3, i.e, the number of independent variables.

The final coded equation generated from Cr(VI) reduction using Cu_2O catalyst based on BBD was found to be well fitted to the quadratic model is:

$$\text{Reduction (Y)} = +84.04 - 13.41A + 26.88B - 7.99C - 6.03AB + 6.20AC - 6.92BC - 11.00A^2 - 28.62B^2 + 5.65C^2 \quad (9)$$

Equation (9) shows how the 3 factors in a quadratic or interactive model affect the Cr(VI) reduction using the Cu_2O catalyst. As shown in equation (9), those with negative coefficients affect Cr(VI) reduction inversely, whereas those with positive coefficients enhance the reduction of Cr(VI). Moreover, the adequacy of the quadratic model to sufficiently explain the Cr(VI) reduction process is validated via statistical parameters such as R^2 and analysis of variance (ANOVA). The detailed ANOVA results of Cr(VI) reduction using Cu_2O nanoparticle catalyst are presented in Table 4.2. As shown in Table 4.2, R^2 (0.9979) is much closer to unity, which implies that the data are well fitted to the quadratic model. In particular, 99.79% of the Cu_2O catalyst reduction of Cr(VI) can be described by the proposed quadratic model (equation (9)).

Table Error! No text of specified style in document.**.4** The analysis of variance (ANOVA) of Cr(VI) reduction based on quadratic model

Source	**Sum of Squares**	**DF**	**Mean Square**	**F-value**	**p-value**	**Fit statistics**
Model	12587.91	9	1398.66	365.94	< 0.0001	SD = 1.96
Residuals	26.75	7	3.82			CV (%) =3.12
Lack of Fit	19.20	3	6.40	3.39	0.1345	R^2 = 0.9979 Predicted R^2 =0.9747
Pure Error	7.55	4	1.89			Adjusted R^2 = 0.9952

Term	**Coefficient estimate**	**Standard error coefficient**	**Mean Square**	**F-value**	**p-value**	**VIF**
Intercept	84.04	0.8743				
A	-13.41	0.6912	1439.16	376.54	< 0.0001	1.0000
B	26.88	0.6912	5778.13	1511.78	< 0.0001	1.0000
C	-7.99	0.6912	510.40	133.54	< 0.0001	1.0000
AB	-6.03	0.9775	145.20	37.99	0.0005	1.0000
AC	6.20	0.9775	153.76	40.23	0.0004	1.0000
BC	-6.92	0.9775	191.82	50.19	0.0002	1.0000
A^2	-11.00	0.9528	509.01	133.18	< 0.0001	1.01
B^2	-28.62	0.9528	3448.86	902.35	< 0.0001	1.01
C^2	-5.65	0.9528	134.17	35.10	0.0006	1.01

The ANOVA in Table 4.2, model F-value of 365.94 implies the quadratic model is significant. There is only a 0.01% chance that an F-value this large could occur due to noise. P-values less than 0.0500 indicate model terms are significant. In this case A, B, C, AB, AC, BC, A^2, B^2, C^2 are significant model terms. The lack of fit F-value of 3.39 implies the Lack of Fit is not significant relative to the pure error. There is a 13.45% chance that a Lack of Fit F-value this large could occur due to noise. Non-significant lack of fit is good ,I want the model to fit. This implies that the Cu_2O nanoparticle reduction of Cr(VI) is well explained by our quadratic model with a 95% confidence level.

The 2-dimensional (2D) and 3-dimensional (3D) surface plots of the response as a function of process variables are useful for a clear understanding of the reaction process. The 2D-3D plots figure 4.6, 4.7, and 4.8 above show the Cr(VI) reduction (%) with varying pH, contact time, and Cr(VI) concentrations, respectively. The reduction (%) of Cr(VI) differs with varying interaction variables and is found to be maximum with AB interaction terms than with AC and BC at a fixed 30 mg Cu_2O nanoparticle. As shown in Figure 4.6 above, the AB interaction optimized at a fixed Cr(VI) concentration (30 mg/L) is the most important interaction parameter in predicting the maximum reduction of Cr(VI).

Figure 4.10 below shows that the predicted R^2 (0.9747) has a reasonable agreement with adjusted R^2 (0.9952), that is, the difference is less than 0.2. It is affirmed that the quadratic model can sufficiently explain the relationship between factors and Cr(VI) reduction (%). Adequate precision (56.580) measures the signal to noise ratio, which is greater than 4 and it indicates an adequate signal. Therefore, the quadratic model can be used to navigate the design space.

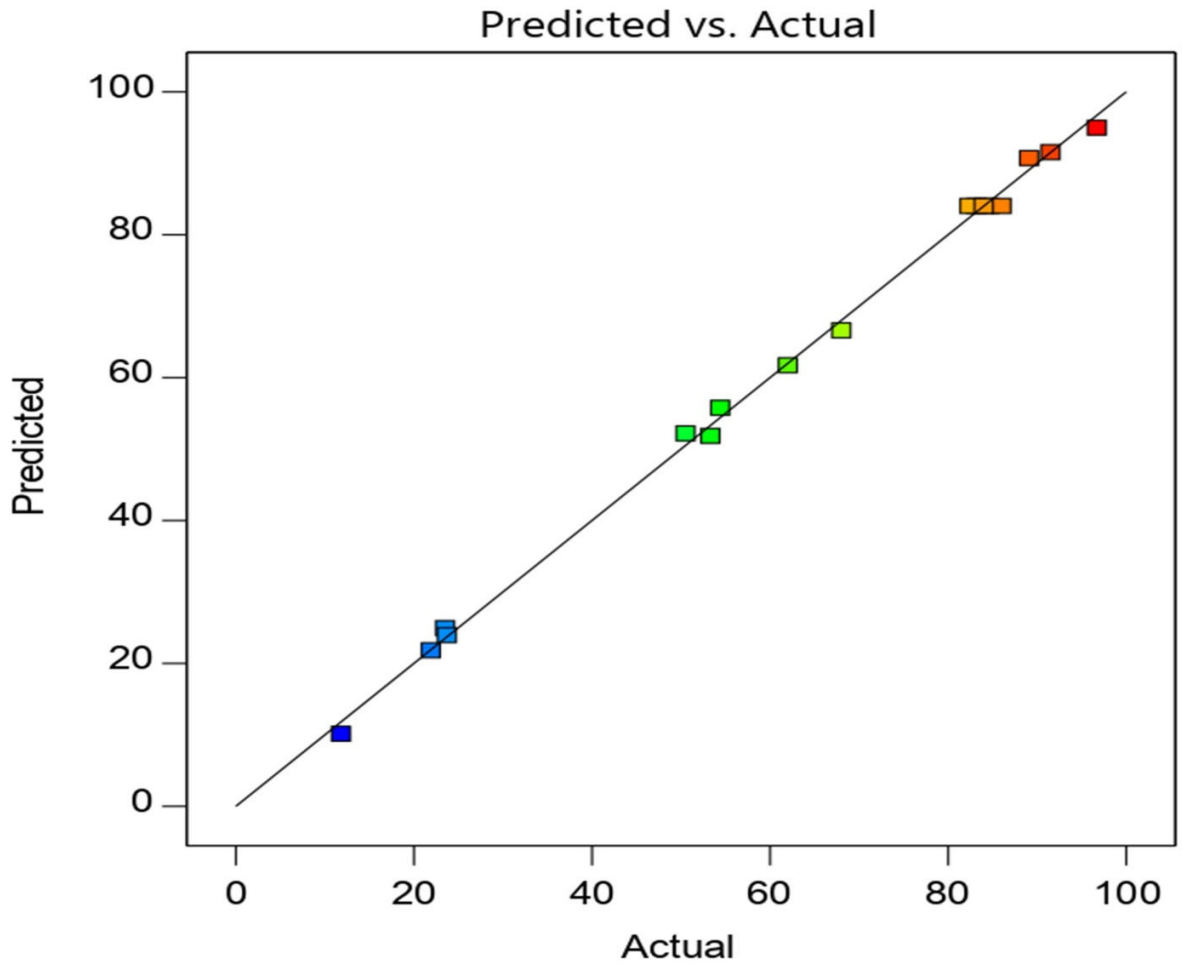

Figure Error! No text of specified style in document.**.19** The comparison of actual (experimental) and model prediction values of Cr (VI) reduction (%).

The RSM-BBD optimization with other scenarios gives maximum reduction of Cr(VI), and based on considering the available resource it is possible to adapt different combinations of pH, contact time, and Cr(VI) concentration. Generally, the numerical optimization of the desired goal is expected to maximize, minimize, in target, be within the range, and be none of the responses and adjust to a precise value for the factors [57]. The numerical optimization found a point that maximizes the desirability function in Cr(VI) reduction. The criteria set for the three factors in the range including pH of the solution (4 - 9), contact time (30 - 180 minutes), and initial Cr(VI) concentration (10 - 50 mg/L) and 99.24% maximum reduction of Cr(VI) were found to be the maximum desirability. Figure 4.11 below shows ramp desirability that was generated from 100 optimum points via numerical optimization.

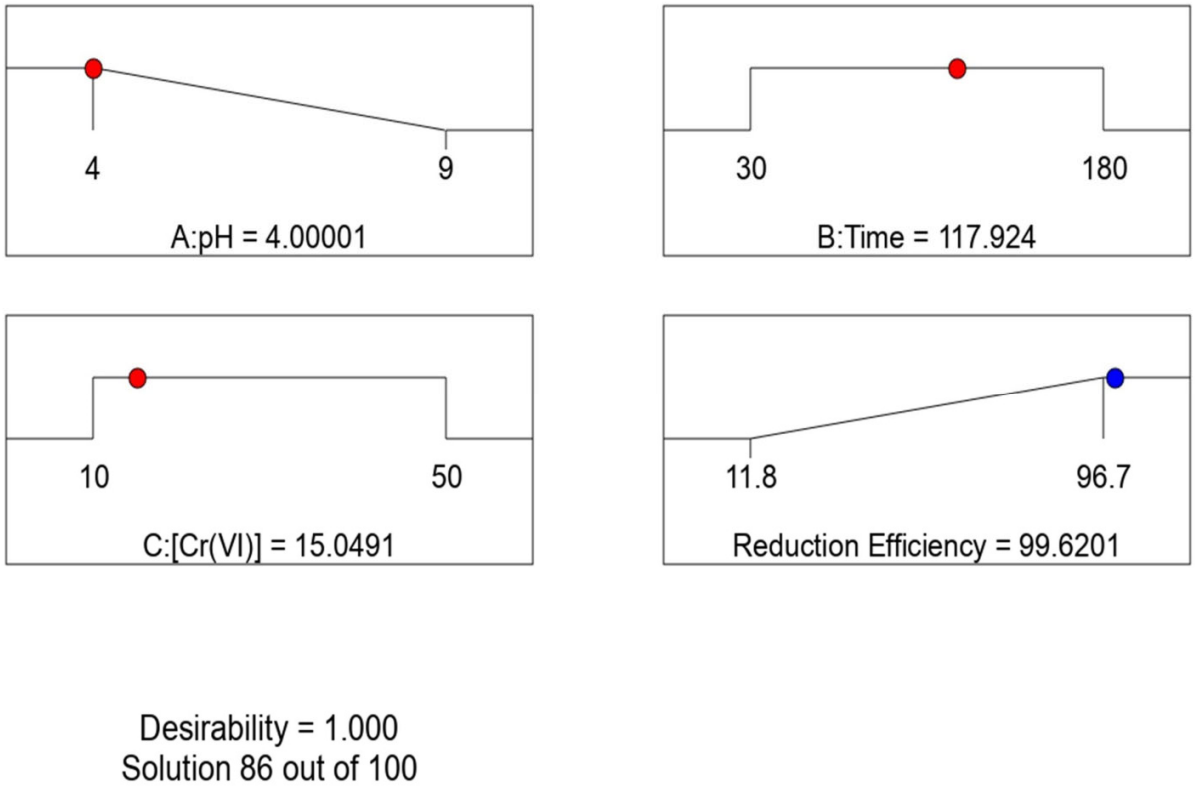

Figure Error! No text of specified style in document..**20** The desirability ramp for optimization of 3 factors (pH solution, contact time, and Cr (VI) concentration) for the maximum reduction (%) of Cr (VI) using Cu_2O nanoparticle.

4.3.6 Reaction mechanism and kinetics of Cr(VI) reduction

The Cu_2O/ visible light nanoparticle show a significant photocatalytic reduction of Cr(VI). This is attributed to the reduction of Cr(VI), which was predominantly through Cu_2O nanoparticle reduction of Cr(VI).

In order to show the possible photocatalytic reduction of dichromate, I conducted a preliminary study to see if the dichromate would not undergo a reduction in direct irradiation in the absence of Cu_2O. The results show that the reduction of hexavalent chromium is negligible during 60 minutes of irradiation .

The absorbance peaks of photocatalytic reduction of Cr(VI) at different time (30, 60, 90, 120 min) have good reduction efficiency at 365 nm as shown in the Figure below 4.12.

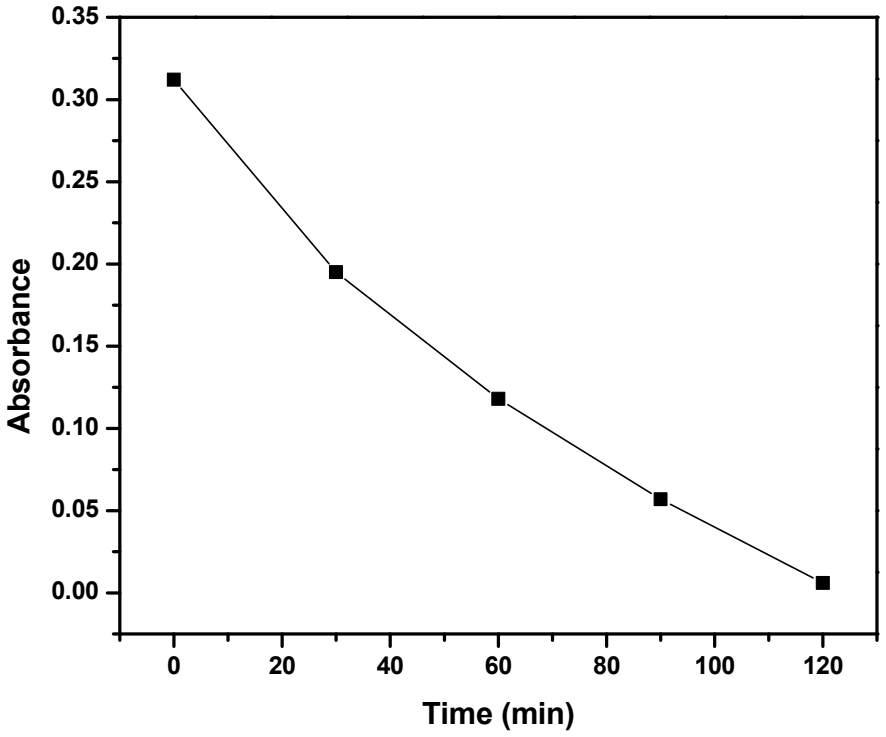

.

Figure Error! No text of specified style in document..**21** Absorbance of photocatalytic reduction of Cr(VI) as a function of time

After 30 min dark adsorption, the photocatalysis process was carried out with Cu_2O photocatalyst. As it is shown in figure 26, Cu_2O can degrade 98.08% of (10 mg/L, 30 mL) at the end of 120 min irradiation. Cu_2O it has poor adsorption capacity, but the photocatalytic activity was observed very good. And a Figure 4.13 below shows a plot of $\ln(C_0/C_t)$ with respect to time gives a straight line whose slope is k_1.

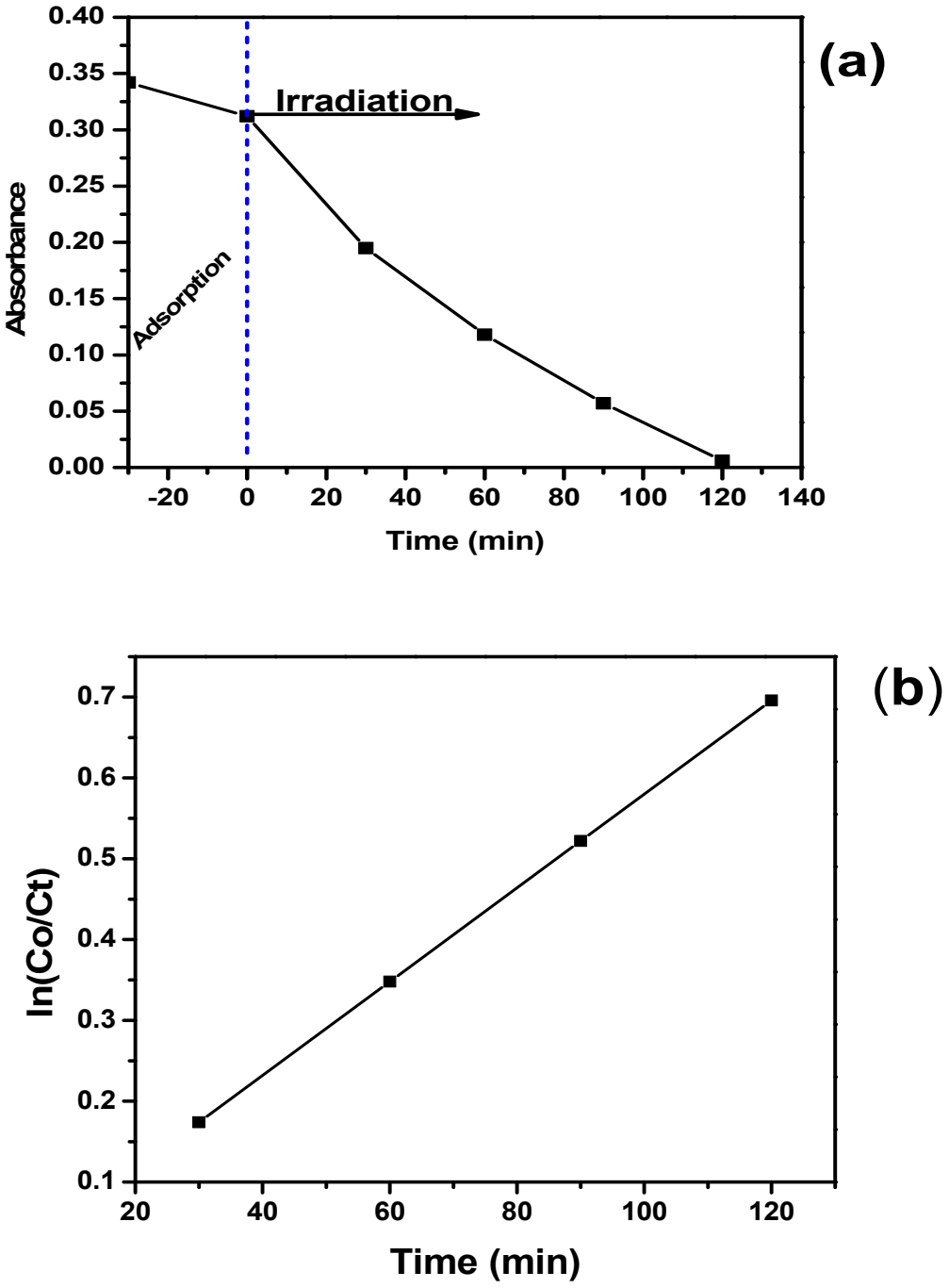

Figure Error! No text of specified style in document..**22** The (a) rate of adsorption and (b) first order ln(Co/Ct) of the Cu_2O/visible light reduction of Cr(VI) to Cr(III) as a function of time

As Figure 4.14 resumes the solution color variation which indicates the modification of toxic Cr(VI) to non-toxic Cr(III) chemical species present in the solution as a function of pH.

A plausible reaction mechanism can be proposed based on the optical characteristics of the Cu_2O photocatalyst. The reaction proceeds to be feasible in terms of the reduction potential of Cr(VI) (E^0 for Cr(VI) / Cr(III) = 1.33 V). With an optical band gap of 2.26 eV, Cu_2O absorbs 400 - 750 nm visible light to generate an electron-hole pair.

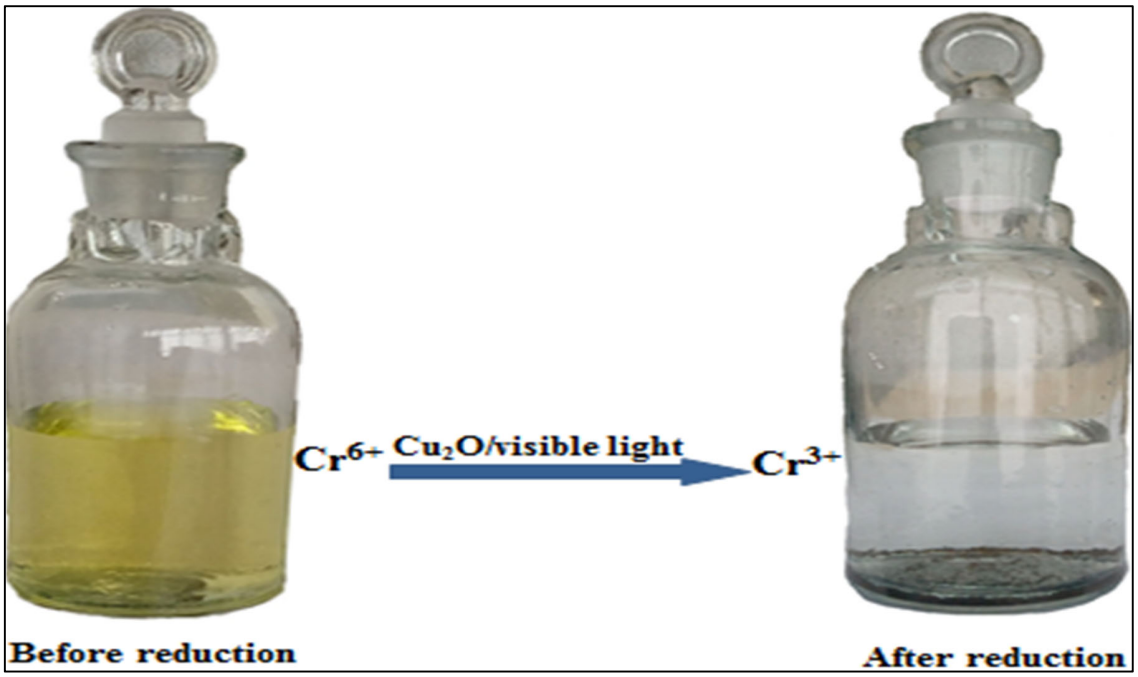

Figure Error! No text of specified style in document..**23** Schema illustrating the color changes of Cr(VI) to Cr(III) at pH=3.

Without a photocatalyst, $K_2Cr_2O_7$ is not degradable under the light irradiation using solar simulator. With Cu_2O as a photocatalyst, however, Cu_2O can absorb photons with energy higher than its band gap, causing electrons to jump across the band gap into conduction band. These free electrons involved in the reactions with the $K_2Cr_2O_7$ solution and Cr^{6+} could be reduced to Cr^{3+} in the form of $Cr(OH)_3$. Similar photocatalytic reduction mechanism was reported by somewhere else [58].

$$Cu_2O + hv\ (visible) \rightarrow Cu_2O\ (e^- + h^+)$$

$$H_2CrO_4 + 6H^+ + 3e^- \rightarrow Cr^{3+} + H_2O$$

$$HCrO4^- + 7H^+ + 3e^- \rightarrow Cr^{3+} + 4H_2O$$

$$Cr_2O_7^{2-} + 14H^+ + 6e^- \rightarrow 2Cr^{3+} + 7H_2O$$

$$CrO_4^{2-} + 8H^+ + 3e^- \rightarrow Cr^{3+} + 4H_2O$$

In this study the photocatalytic reduction of Cr(VI) to Cr(III) takes place when a Cr(VI) solution containing Cu_2O is illuminated in visible light having photon energy greater than the band gap energy of the semiconductor. During photocatalysis, reduction occurs first when Cu_2O is dispersed in the aqueous solution containing metal ions. The reduction of Cr(VI) to Cr(III) occurs because, under illumination, electron-hole pairs are created inside the semiconductor particles.

$$Cu_2O + hv\ (visible) \longrightarrow Cu_2O\ (h^+_{VB} + e^-_{CB})$$

After the migration of these species to the surface of the particles, the photogenerated electrons reduce Cr(VI) to Cr(III) and the holes oxidize water and the sacrificial electron donor.

In acidic medium, $Cr_2O_7^{2-} + 14\ H^+ + 6\ e^- \longrightarrow 2Cr^{3+} + 7H_2O$

In alkaline medium, $Cr_2O_7^{-2} + 14H_2O + 3e^- \longrightarrow Cr(OH)_3 + 5OH^-$

$$2H_2O + h^+ \longrightarrow 4H^+ + O_2$$

Photocatalysis involves capturing of photons by a semiconductor such as cuprous oxide (Cu_2O), resulting in the creation of electrons and positive holes and subsequent redox reactions as shown below in Figure 4.15.

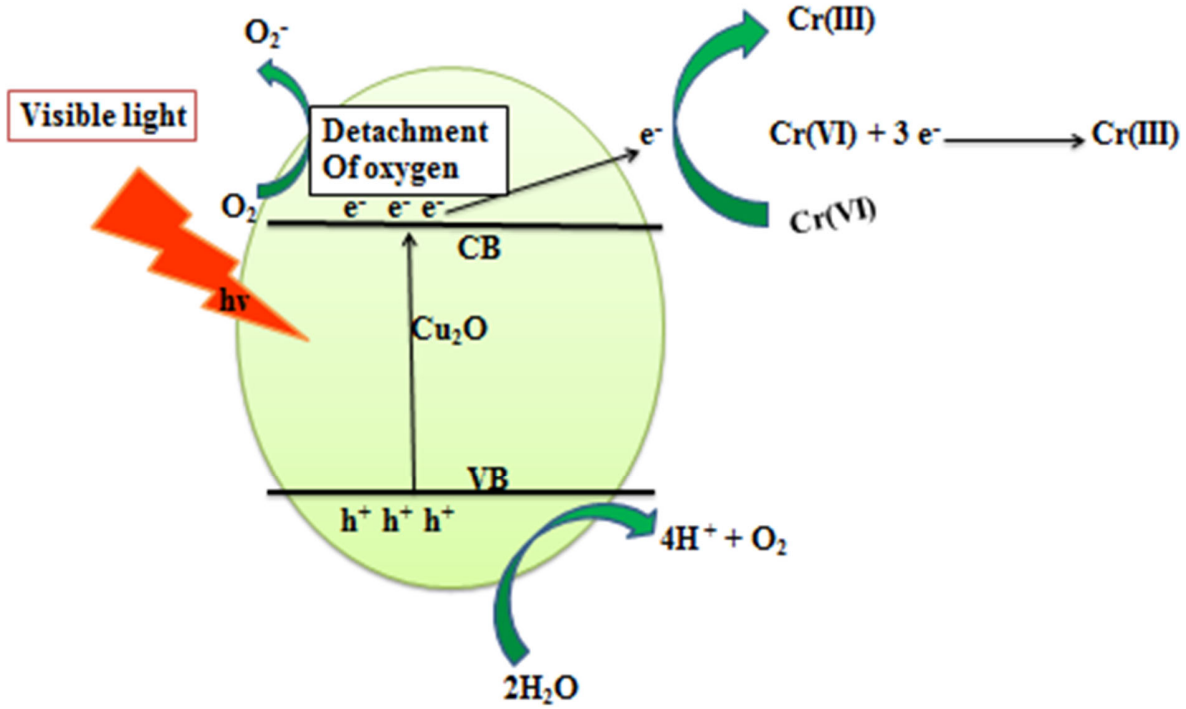

Figure Error! No text of specified style in document..**24** A simplified schematic reaction mechanism for photocatalytic reduction of Cr(VI) with Cu_2O photocatalysis process

5 CONCLUSION

In conclusion, Cu2O nanoparticle was synthesized using *prunus cerasifera* as reducing agent in an aqueous medium. FT-IR and XRD pattern confirms formation of Cu_2O nanoparticle. Red-shift in the Cu–O stretching vibrational band in presence of plant extract confirms surface interaction between Cu_2O nanoparticle and *Prunus cerasifera*. The Cu_2O nanoparticle is effective for photocatalytic reduction of hexavalent chromium under visible light has been demonstrated. The reduction efficiency of Cr(VI) was higher in acidic solutions than that in alkaline solutions. .The most important photocatalytic reduction of hexavalent chromium parameters (such as pH, contact time, and concentrations of Cr(VI)) were optimized using RSM-BBD. A 3-level quadratic model can effectively show the interaction of parameters. This was validated by both regression (R^2 = 0.9979 and adjusted R^2 = 0.9952) and ANOVA ($P < .0001$) analyses. The optimum conditions for maximum % reduction was found to 99.24 % at 115 min, 12.56 mg/L Cr (VI), and pH =4.0. Reduction process kinetics obey first order kinetic model. Heavy metal ions and organic pollutants often present in real wastewater, this research suggests that the photocatalytic reaction Cu_2O could be applied to more effectively treat wastewaters containing both Cr (VI) and organic compounds than those containing a single species only.

REFERENCES

1. Bleeker, E.A.J., *Considerations on the EU definition of a nanomaterial: Science to support policy making.* Regulatory Toxicology and Pharmacology, 2013. **65**: p. 119-125.
2. Alagarasi, A., *Introduction to nanomaterials.* 2011: p. 1-25.
3. Nemerow, N.L. and A. Dasgupta, *Industrial and hazardous waste treatment.* 1991.
4. Rahman, Z. and V.P. Singh, *The relative impact of toxic heavy metals (THMs)(arsenic (As), cadmium (Cd), chromium (Cr)(VI), mercury (Hg), and lead (Pb)) on the total environment: an overview.* Environmental monitoring and assessment, 2019. **191**(7): p. 1-21.
5. Tchounwou, P.B., et al., *Heavy metal toxicity and the environment.* Molecular, clinical and environmental toxicology, 2012: p. 133-164.
6. Registry, A.A.f.T.S.a.D., *Substance Priority List.* 1999.
7. R.Beaglehole, R.B., T.Kjellstorm, *Basic epidemiology.* 1993.
8. Peter Dobson, S.K., *Nanoparticle.* 2019.
9. Saleh, T.A., *Nanomaterials: Classification, properties, and environmental toxicities.* Environmental Technology & Innovation, 2020. **20**: p. 101067.
10. Tran, P.D., et al., *A cuprous oxide–reduced graphene oxide (Cu 2 O–rGO) composite photocatalyst for hydrogen generation: employing rGO as an electron acceptor to enhance the photocatalytic activity and stability of Cu 2 O.* Nanoscale, 2012. **4**(13): p. 3875-3878.
11. Yue, Y., et al., *Enhanced dark adsorption and visible-light-driven photocatalytic properties of narrower-band-gap Cu2S decorated Cu2O nanocomposites for efficient removal of organic pollutants.* Journal of hazardous materials, 2020. **384**: p. 121302.
12. Yu, Z., et al., *Epitaxial growth and microstructure of Cu2O nanoparticle/thin films on SrTiO3 (100).* Nanotechnology, 2007. **18**(11): p. 115601.
13. Filippetti, A. and V. Fiorentini, *Coexistence of ionic and metallic bonding in noble-metal oxides.* Physical Review B, 2005. **72**(3): p. 035128.
14. *Copper (I) Oxide - Structure, Properties and Uses*
15. A. Filippetti, V.F., *Coexistence of ionic and metallic bonding in noble-metal oxides,.* Physical review B., 2005. **72**(3): p. 1-8.
16. Suvaci, E.Ö., Emel, *Hydrothermal Synthesis*, in *Reference Module in Materials Science and Materials Engineering*. 2020, Elsevier.
17. Mayur Valodkar, A.P., Sonal Thakore, *Synthesis and characterization of cuprous oxide dendrites: New simplified green hydrothermal route.* Journal of Alloys and Compounds, 2011. **509**(2): p. 523-528.
18. Gennari, F.C. and J.J. Andrade-Gamboa, *Chapter 13 - A Systematic Approach to the Synthesis, Thermal Stability and Hydrogen Storage Properties of Rare-Earth Borohydrides*, in *Emerging Materials for Energy Conversion and Storage*, K.Y. Cheong, G. Impellizzeri, and M.A. Fraga, Editors. 2018, Elsevier. p. 429-459.
19. Chen, D., et al., *Preparation of Cu2O nanoparticles in cupric chloride solutions with a simple mechanochemical approach.* Journal of Alloys and Compounds, 2010. **504**: p. S345-S348.
20. Soytaş, S.H., O. Oğuz, and Y.Z. Menceloğlu, *9 - Polymer Nanocomposites With Decorated Metal Oxides*, in *Polymer Composites with Functionalized Nanoparticles*, K. Pielichowski and T.M. Majka, Editors. 2019, Elsevier. p. 287-323.
21. Athar, T., *Chapter 17 - Smart precursors for smart nanoparticles*, in *Emerging Nanotechnologies for Manufacturing (Second Edition)*, W. Ahmed and M.J. Jackson, Editors. 2015, William Andrew Publishing: Boston. p. 444-538.

22. Pintor Simamora, J.R.S., and Berton M. Siahaan, *Synthesis and characterization optical properties of cu2o nanoparticles with coprecipitation method based concentration variations precipitator.* Trends in Science and Science Education, 2014: p. 249-259.
23. Schubert, U., *7.10 - Sol–Gel Processing of Metal Compounds*, in *Comprehensive Coordination Chemistry II*, J.A. McCleverty and T.J. Meyer, Editors. 2003, Pergamon: Oxford. p. 629-656.
24. Livage, J., *Basic principles of sol-gel chemistry.*
25. Zayyoun, N.B., L. Laânab, L. Jaber, B., *The effect of pH on the synthesis of stable Cu_2O/CuO nanoparticles by sol–gel method in a glycolic medium.* Applied Physics A, 2016. **122**(5): p. 488.
26. Halin, D., et al., *EFFECT OF SPIN COATING RATE ON MORPHOLOGY AND OPTICAL PROPERTIES OF CUPROUS OXIDE THIN FILM PREPARED BY SOL-GEL TECHNIQUE.* Journal of the Australasian Ceramic Society, 2010. **46**(1): p. 41-45.
27. Basu, P., *Chapter 4 - Torrefaction*, in *Biomass Gasification, Pyrolysis and Torrefaction (Third Edition)*, P. Basu, Editor. 2018, Academic Press. p. 93-154.
28. Seekaew, Y., et al., *Chapter Nine - Synthesis, Characterization, and Applications of Graphene and Derivatives*, in *Carbon-Based Nanofillers and Their Rubber Nanocomposites*, S. Yaragalla, et al., Editors. 2019, Elsevier. p. 259-283.
29. Curnutte, B., *Principles of Microwave Radiation.* J Food Prot, 1980. **43**(8): p. 618-624.
30. Zhang, H., et al., *Microwave-assisted synthesis of Cu2O microcrystals with systematic shape evolution from octahedral to cubic and their comparative photocatalytic activities.* RSC Advances, 2014. **4**(72): p. 38059-38063.
31. Monica Debbarma, P.S., Mitali Saha, *Synthesis of Cu_2O nanoparticles and current–voltage measurements (I-V) of its nanocomposites.* Nanotechenology.Environmental Engineering, 2016. **1**(6).
32. Banik, B.K. and B.M. Sahoo, *19 - Green synthesis and biological evaluation of anticancer drugs*, in *Green Approaches in Medicinal Chemistry for Sustainable Drug Design*, B.K. Banik, Editor. 2020, Elsevier. p. 651-712.
33. Singh, J., et al., *'Green' synthesis of metals and their oxide nanoparticles: applications for environmental remediation.* Journal of Nanobiotechnology, 2018. **16**(1): p. 84.
34. Shaheen Pathan, S.K., Divya Marolikar, Harsha Mishra, Shweta Nadar, Muskan Jha, *Green synthesis and characterization of cuprous oxide nanoparticles using tea extract.* 2nd International Conference on Advances in Science & Technology, 2019: p. 1-3.
35. Behera, M. and G. Giri, *Green synthesis and characterization of cuprous oxide nanoparticles in presence of a bio-surfactant.* Materials Science-Poland, 2014. **32**(4): p. 702-708.
36. Preeti Birwal1, D.G., Saurabh SP[1] and Pragati S[2], *Plums: A Brief Introduction.* Journal of Food, Nutrition and Population Health, 2017. **1**: p. 1-8.
37. *The Health Benefits of Prunes & Plums.*
38. Preeti Birwal1, D.G., Saurabh SP and Pragati S, *Plums: A Brief Introduction.* Journal of Food, Nutrition and Population Health, 2017. **1**(1:8): p. 1-5.
39. Shipp, J., & Abdel-Aal, E. S. M, *Food applications and physiological effects of anthocyanins as functional food ingredients.* The open food science journal, 2010. **4**(1): p. 7-22.
40. Vanini, L.S., Hirata, T. A., Kwiatkowski, A., & Clemente, E, *Extraction and stability of anthocyanins from the benitaka grape cultivar (Vitis vinifera L.).* Brazilian journal of food technology, 2009. **12**(3): p. 213-219.

41. Naira Nayeem, A.S., Heba Sale1 and Said AHEl-Alfqy, *Gallic Acid: A Promising Lead Molecule for Drug Development.* Journal of Applied Pharmacy, 2016. **8**(2): p. 1-4.
42. Tang HR, C.A., Hancock RA, *Structure-activity relationships in the hydrophobic interactions of polyphenols with cellulose and collagen.* Biopolymers, 2003. **70**: p. 403-413.
43. Nikolic, K.M., *Theoretical study of phenolic antioxidants properties in reaction with oxygen-centered radicals.* Journal of molecular structure: THEOCHEM, 2006. **774**(1-3): p. 95-105.
44. Shahriar K, R.J., *Monocyclic Phenolic Acids; Hydroxy- and Polyhydroxybenzoic Acids: Occurrence and Recent Bioactivity Studies.* Molecules, 2010. **15**: p. 7985-8005.
45. Wang W, A.A., Abualnaja KO, Covaci A, Gevao B, *Synthetic phenolic antioxidants and their metabolites in indoor dust from homes and microenvironments.* Environmental Science & Technology, 2016. **50**(1): p. 428-434.
46. Yadav, S., A. Jain, and P. Malhotra, *A review on the sustainable routes for the synthesis and applications of cuprous oxide nanoparticles and their nanocomposites.* Green Chemistry, 2019. **21**(5): p. 937-955.
47. Shupack*, S., *The Chemistry of Chromium and Some Resulting Analytical Problems.* Environmental Health Perspectives, 1991. **92**: p. 7-11.
48. From Wikipedia, t.f.e., *Chromate and dichromate.*
49. Bharagava, R.N. and S. Mishra, *Hexavalent chromium reduction potential of Cellulosimicrobium sp. isolated from common effluent treatment plant of tannery industries.* Ecotoxicology and Environmental Safety, 2018. **147**: p. 102-109.
50. Mehdi Shirzad-Siboni, M.F., Reza Darvishi Cheshmeh Soltani, Alireza Khataee, and Sama Tajassosi, *Photocatalytic Reduction of Hexavalent Chromium over ZnO Nanorods Immobilized on Kaolin.* Industrial & Engineering Chemistry Research, 2014. **53**: p. 1079-1087.
51. Gheju, M. and A. Iovi, *Kinetics of hexavalent chromium reduction by scrap iron.* Journal of hazardous materials, 2006. **135**(1-3): p. 66-73.
52. Williams, A.G. and M.M. Scherer, *Kinetics of Cr (VI) reduction by carbonate green rust.* Environmental Science & Technology, 2001. **35**(17): p. 3488-3494.
53. Nakamoto, K. and A.E. Martell, *Infrared Spectra of Metal-Chelate Compounds. I. A Normal Coordinate Treatment on Bis-(Acetylacetonato)-Cu (II).* The Journal of Chemical Physics, 1960. **32**(2): p. 588-597.
54. Gasque, L., et al., *Cu–O stretching frequency correlation with phenanthroline pKa values in mixed copper complexes.* Inorganica chimica acta, 1999. **288**(1): p. 106-111.
55. McNeil, S.E., *Characterization of nanoparticles intended for drug delivery*. Vol. 697. 2011: Springer.
56. Clogston, J.D. and A.K. Patri, *Zeta potential measurement*, in *Characterization of nanoparticles intended for drug delivery*. 2011, Springer. p. 63-70.
57. Neway Belachew , R.F.a.A.A.A., *RSM-BBD Optimization of Fenton-Like Degradation of 4-Nitrophenol Using Magnetite Impregnated Kaolin.* Air, Soil and Water Research, 2020. **13**: p. 1-10.
58. Loryuenyong, V.J., Natnapin Chuangchai, Thirawich Buasri, Achanai, *The Photocatalytic Reduction of Hexavalent Chromium by Controllable Mesoporous Anatase TiO_2 Nanoparticles.* Advances in Materials Science and Engineering, 2014. **2014**: p. 8 pages.

APPENDIXES

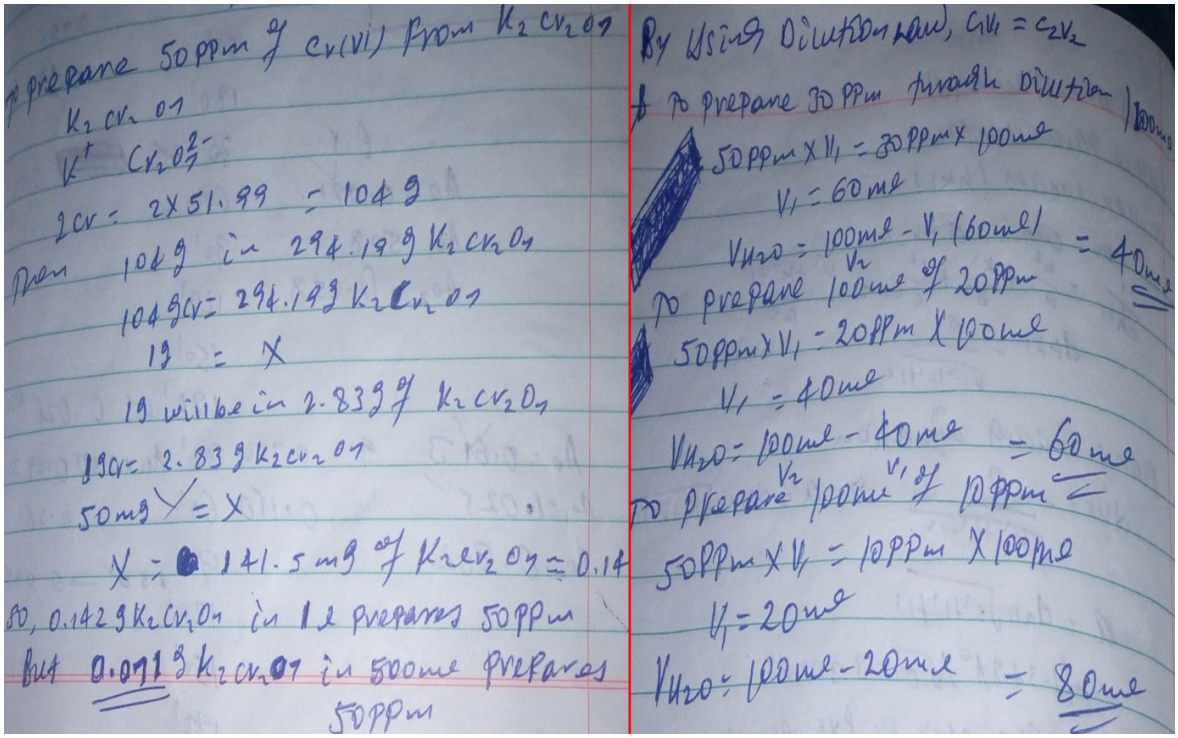

Box-Behnken Design

Std	Run	Factor 1 A:pH	Factor 2 B:Time (min)	Factor 3 C:Concenteration (mg/L)	Response 1 Reduction Effic. (%)
8	1	9	105	50	50.5
15	2	6.5	105	30	82.4
3	3	4	180	30	89.1
12	4	6.5	180	50	62
9	5	6.5	30	10	23.7
14	6	6.5	105	30	84.6
1	7	4	30	30	23.5
5	8	4	105	10	96.7
16	9	6.5	105	30	86
6	10	9	105	10	54.4
11	11	6.5	30	50	21.9
13	12	6.5	105	30	83.2
10	13	6.5	180	10	91.5
2	14	9	30	30	11.8
7	15	4	105	50	68
17	16	6.5	105	30	84
4	17	9	180	30	53.3

Build Information

File Version	11.1.0.1		
Study Type	Response Surface	**Subtype**	Randomized
Design Type	Box-Behnken	**Runs**	17
Design Model	Quadratic	**Blocks**	No Blocks
Build Time (ms)	2.00		

Model Terms

Term	Standard Error*	VIF	R_i^2	Power
A	0.3536	1	0.0000	68.1 %
B	0.3536	1	0.0000	68.1 %
C	0.3536	1	0.0000	68.1 %
AB	0.5000	1	0.0000	40.8 %
AC	0.5000	1	0.0000	40.8 %
BC	0.5000	1	0.0000	40.8 %
A^2	0.4873	1.00588	0.0058	93.8 %
B^2	0.4873	1.00588	0.0058	93.8 %
C^2	0.4873	1.00588	0.0058	93.8 %

- For a standard deviation of 1.

Response 1: Reduction Efficiency

Source	Sequential p-value	Lack of Fit p-value	Adjusted R^2	Predicted R^2	
Linear	0.0052	< 0.0001	0.5232	0.3630	
2FI	0.7750	< 0.0001	0.4424	-0.0673	
Quadratic	**< 0.0001**	**0.1345**	**0.9952**	**0.9747**	**Suggested**
Cubic	0.1345		0.9976		Aliased

Final Equation in Terms of Coded Factors

Reduction Efficiency	=
+84.04	
-13.41	A
+26.88	B
-7.99	C
-6.03	AB
+6.20	AC
-6.92	BC
-11.00	A^2
-28.62	B^2
-5.65	C^2

Calibration curve for reduction kinetics	
[Cr(VI)] (mg/L)	**Abs**
10	**0.357**
30	**0.977**
50	**1.629**

ANOVA for Quadratic model

Response 1: Reduction Efficiency

Source	Sum of Squares	Df	Mean Square	F-value	p-value	
Model	12587.91	9	1398.66	365.94	< 0.0001	Significant
A-Ph	1439.16	1	1439.16	376.54	< 0.0001	
B-Contact Time	5778.13	1	5778.13	1511.78	< 0.0001	
C-Concenteration	510.40	1	510.40	133.54	< 0.0001	
AB	145.20	1	145.20	37.99	0.0005	
AC	153.76	1	153.76	40.23	0.0004	
BC	191.82	1	191.82	50.19	0.0002	
A^2	509.01	1	509.01	133.18	< 0.0001	
B^2	3448.86	1	3448.86	902.35	< 0.0001	
C^2	134.17	1	134.17	35.10	0.0006	
Residual	26.75	7	3.82			
Lack of Fit	19.20	3	6.40	3.39	0.1345	not significant
Pure Error	7.55	4	1.89			
Cor Total	12614.66	16				

Fit Statistics

Std. Dev.	1.96		R^2	0.9979
Mean	62.74		Adjusted R^2	0.9952
C.V. %	3.12		Predicted R^2	0.9747
			Adeq Precision	56.5800

Coefficients in Terms of Coded Factors

Factor	Coefficient Estimate	Df	Standard Error	95% CI Low	95% CI High	VIF
Intercept	84.04	1	0.8743	81.97	86.11	
A-Ph	-13.41	1	0.6912	-15.05	-11.78	1.0000
B-Contact Time	26.88	1	0.6912	25.24	28.51	1.0000
C-Concenteration	-7.99	1	0.6912	-9.62	-6.35	1.0000
AB	-6.03	1	0.9775	-8.34	-3.71	1.0000
AC	6.20	1	0.9775	3.89	8.51	1.0000
BC	-6.92	1	0.9775	-9.24	-4.61	1.0000
A^2	-11.00	1	0.9528	-13.25	-8.74	1.01
B^2	-28.62	1	0.9528	-30.87	-26.37	1.01
C^2	-5.65	1	0.9528	-7.90	-3.39	1.01

Report

Run Order	Actual Value	Predicted Value	Residual	Leverage	Internally Studentized Residuals	Externally Studentized Residuals	Cook's Distance	Influence on Fitted Value DFFITS	Standard Order
1	50.50	52.20	-1.70	0.750	-1.739	-2.137	0.907	-3.701[1]	8
2	82.40	84.04	-1.64	0.200	-0.938	-0.929	0.022	-0.464	15
3	89.10	90.74	-1.64	0.750	-1.675	-2.004	0.842	-3.471[1]	3
4	62.00	61.74	0.2625	0.750	0.269	0.250	0.022	0.433	12
5	23.70	23.96	-0.2625	0.750	-0.269	-0.250	0.022	-0.433	9
6	84.60	84.04	0.5600	0.200	0.320	0.299	0.003	0.149	14
7	23.50	24.94	-1.44	0.750	-1.471	-1.638	0.649	-2.837[1]	1
8	96.70	95.00	1.70	0.750	1.739	2.137	0.907	3.701[1]	5
9	86.00	84.04	1.96	0.200	1.121	1.146	0.031	0.573	16
10	54.40	55.77	-1.37	0.750	-1.407	-1.538	0.594	-2.663[1]	6
11	21.90	21.84	0.0625	0.750	0.064	0.059	0.001	0.103	11
12	83.20	84.04	-0.8400	0.200	-0.480	-0.452	0.006	-0.226	13
13	91.50	91.56	-0.0625	0.750	-0.064	-0.059	0.001	-0.103	10
14	11.80	10.16	1.64	0.750	1.675	2.004	0.842	3.471[1]	2
15	68.00	66.62	1.38	0.750	1.407	1.538	0.594	2.663[1]	7
16	84.00	84.04	-0.0400	0.200	-0.023	-0.021	0.000	-0.011	17
17	53.30	51.86	1.44	0.750	1.471	1.638	0.649	2.837[1]	4

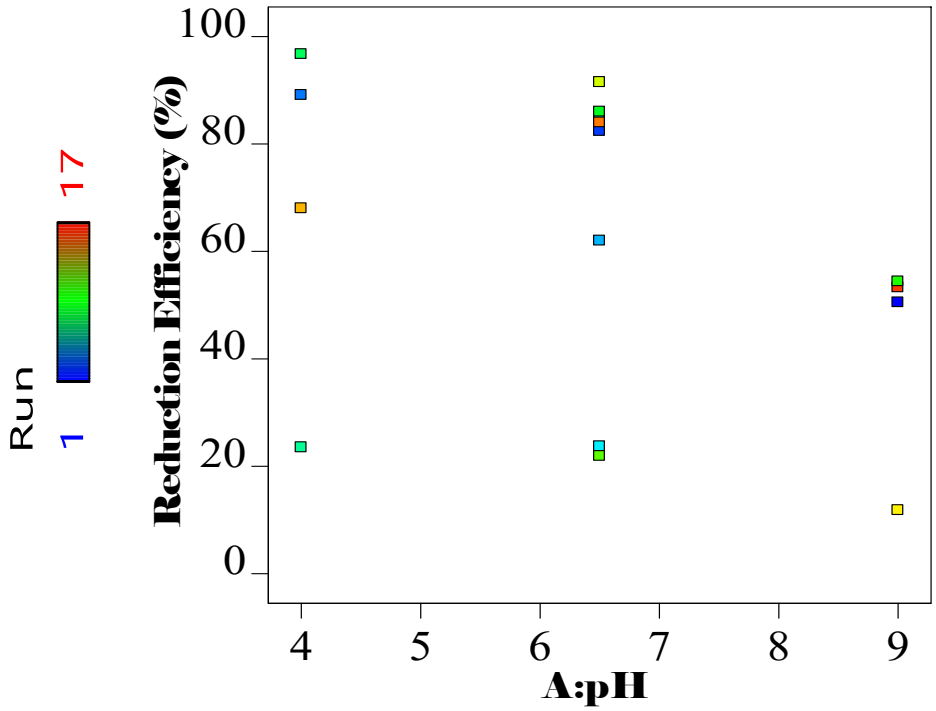

Factors

Factor	Name	Units	Type	Minimum	Maximum	Coded Low	Coded High	Mean	Std. Dev.
A	pH		Numeric	4.00	9.00	-1 ↔ 4.00	+1 ↔ 9.00	6.50	1.77
B	Contact Time	min	Numeric	30.00	180.00	-1 ↔ 30.00	+1 ↔ 180.00	105.00	53.03
C	Concenteration	mg/L	Numeric	10.00	50.00	-1 ↔ 10.00	+1 ↔ 50.00	30.00	14.14